Bulletin of the Seismological Society of America, Vol. 92, No. 8, pp. 3042–3066, December 2002

3D Heterogeneous Staggered-Grid Finite-Difference Modeling of Seismic Motion with Volume Harmonic and Arithmetic Averaging of Elastic Moduli and Densities

by Peter Moczo, Jozef Kristek, Václav Vavryčuk, Ralph J. Archuleta, and Ladislav Halada

Abstract We analyze the problem of a heterogeneous formulation of the equation of motion and propose a new 3D fourth-order staggered-grid finite-difference (FD) scheme for modeling seismic motion and seismic-wave propagation.

We first consider a 1D problem for a welded planar interface of two half-spaces. A simple physical model of the contact of two media and mathematical considerations are shown to give an averaged medium representing the contact of two media. An exact heterogeneous formulation of the equation of motion is a basis for constructing the corresponding heterogeneous FD scheme.

In a much more complicated 3D problem we analyze a planar-interface contact of two isotropic media (both with interface parallel to a coordinate plane and interface in general position in the Cartesian coordinate system) and a nonplanar-interface contact of two isotropic media. Because in the latter case 21 elastic coefficients at each point are necessary to describe the averaged medium, we consider simplified boundary conditions for which the averaged medium can be described by only two elastic coefficients.

Based on the simplified approach we construct the explicit heterogeneous 3D fourth-order displacement-stress FD scheme on a staggered grid with the volume harmonic averaging of the shear modulus in grid positions of the stress-tensor components, volume harmonic averaging of the bulk modulus in grid positions of the normal stress-tensor components, and volume arithmetic averaging of density in grid positions of the displacement components.

Our displacement-stress FD scheme can be easily modified into the velocity-stress or displacement-velocity-stress FD schemes.

The scheme allows for an arbitrary position of the material discontinuity in the spatial grid. Numerical tests for 12 configurations in four types of models show that our scheme is more accurate than the staggered-grid schemes used so far.

Numerical examples also show that differences in thickness of a soft surface or interior layer smaller than one grid spacing can cause considerable changes in seismic motion. The results thus underline the importance of having a FD scheme with sufficient sensitivity to heterogeneity of the medium.

Introduction

The finite-difference (FD) method is the dominant method in recent numerical 3D modeling of earthquake ground motion. The main reason is its robustness: the method is applicable to complex models of the Earth's interior and, at the same time, relatively accurate and computationally efficient. Moreover, it is relatively simple and easy to implement in the computer codes. It is appropriate to use the word "relatively" because neither the FD method is free of inherent limitations nor is its application to complex models fully elaborated. Being aware of this, we are far from claiming that the FD method is the best method. It has, however, advantages compared to other methods in many practical applications. For good comparison with other methods we refer to Takenaka *et al.* (1998) and Mizutami *et al.* (2000).

The key role of the FD method in recent earthquake ground motion modeling is evident from numerous recent studies—for example, Olsen and Schuster (1992), Frankel

(1993), Yomogida and Etgen (1993), Graves (1993), Olsen *et al.* (1995), Pitarka *et al.* (1997, 1998), Wald and Graves (1998), Graves *et al.* (1998), Matsushima *et al.* (1998), Cotton *et al.* (1998), Kristek *et al.* (1999), Aoi and Fujiwara (1999), Olsen *et al.* (2000), and Frankel and Stephenson (2000).

The equation of motion for an isotropic medium can be formulated in several ways. Four basic and natural formulations are in displacement-stress, displacement-velocity-stress, velocity-stress, and displacement (see, e.g., Moczo *et al.*, 2001). Given different formulations of the equation of motion and different types of spatial/temporal grids and FD approximations, it is obvious that, in principle, one can construct a variety of the FD schemes to solve one particular problem. Because they differ from one another by accuracy and efficiency, the schemes are not equally good for solving the problem.

Generally, there are explicit and implicit FD schemes. In the explicit schemes, the motion at a given spatial grid point and time level is calculated only from the motion at previous time levels and material parameters. In the implicit schemes, the motion at a given time level is calculated simultaneously at all spatial grid points from the motion at previous time levels and material parameters using an inverse matrix. As pointed out, for example, by Kelly *et al.* (1976), the explicit schemes are computationally simpler. All recent earthquake ground-motion modeling studies use the explicit schemes.

Motion in a smoothly heterogeneous elastic continuum is governed by the equation of motion. The equation can be solved by a proper FD scheme, and very good accuracy can be achieved at a reasonable price—see, for example, the optimized FD schemes developed by Geller and Takeuchi (1998) and Takeuchi and Geller (2000).

Models of the Earth's interior and surface geological structures have to include layers/blocks of different materials and thus also interfaces between them. If the medium contains a material discontinuity, that is, an interface between two homogeneous or smoothly heterogeneous media, at which density and elastic moduli change discontinuously, the equation of motion still governs motion outside the discontinuity but boundary conditions apply at the discontinuity. Then a natural approach to use the FD method is to apply (1) a FD scheme for the smoothly heterogeneous medium at grid points outside the discontinuity, (2) a FD scheme obtained by a proper discretization of the boundary conditions at grid points at or near the discontinuity. This approach is called homogeneous. As already stressed by Boore (1972) and Kelly *et al.* (1976), a homogeneous FD scheme is specific for a particuar problem. Although it may be suitable for simple geometry of discontinuities, its application to complex models with curved material discontinuities is difficult and therefore impractical. In any case, the approach requires stable and sufficiently accurate FD approximation to the boundary conditions, which is not a trivial problem.

In the alternative heterogeneous approach, only one FD scheme is used for all interior grid points (points not lying on boundaries of a grid) no matter what their positions are with respect to the material discontinuity. The presence of the material discontinuity is accounted for only by values of elastic moduli and density. Therefore, the heterogeneous approach has been much more popular since the beginning of seventies. There are, however, two fundamental questions in the heterogeneous approach: (1) Is the heterogeneous approach justified? In other words, is it possible to find a heterogeneous formulation of the equation of motion? (2) How are the values of the material parameters at grid points at and near the discontinuity determined? Strictly speaking, the second question has sense only if there is a positive answer to the first question.

Let us very briefly review how different authors addressed the problem of a material discontinuity and the two aforementioned questions.

In their pioneering work, Alterman and Karal (1968) used the displacement FD scheme and homogeneous approach for models with simple geometry of the material discontinuities. They introduced concept of fictitious grid points in order to approximate boundary conditions on material discontinuities.

Difficulties in application of the homogeneous approach to curved discontinuities led Boore (1972) to his explicit continuous stress method. Boore tried to explicitly include stress-continuity condition on discontinuities differently from the homogeneous and heterogeneous approaches. Due to poor numerical properties of the method, Boore (1972) applied the heterogeneous approach in his *SH* modeling. In order to follow detailed variation of the torsion modulus he calculated effective grid moduli as integral harmonic averages along grid lines between two neighboring grid points, as suggested by Tikhonov and Samarskii (see, e.g., Mitchell, 1969, p. 23).

Ilan *et al.* (1975) and Ilan and Loeventhal (1976) solved the *P-SV* problem on the horizontal and vertical planar discontinuities with the homogeneous approach. Instead of the fictitious grid points they used Taylor expansions of displacement to couple the equation of motion with the boundary conditions.

Kelly *et al.* (1976) presented their heterogeneous *P-SV* schemes with simple intuitive averaging of material parameters. They compared the heterogeneous and homogeneous formulations using numerical tests and showed unacceptable difference between the two approaches in the case of the corner-edge model.

Kummer and Behle (1982) followed the approach of Ilan *et al.* (1975) and derived the second-order *SH* schemes for different types of grid points lying on the steplike polygonal discontinuity between two homogeneous blocks.

A major step forward in the FD modeling of seismic wave propagation in heterogeneous media was done by Virieux (1984, 1986), who used the idea of the staggered grid (Madariaga, 1976). Although Virieux did not say explicitly how he determined material grid parameters in his hetero-

geneous second-order *SH* and *P-SV* velocity-stress schemes, his numerical results were sufficiently accurate at the time. Moreover, the accuracy of the staggered-grid schemes did not suffer from large values of Poisson's ratio, which was the case of all displacement schemes on conventional grids. Virieux also discussed the discrepancy between the homogeneous and heterogeneous formulations found by Kelly *et al.* (1976). He found it difficult to explain features of the homogeneous solution. We consider this a likely indication of a problem to find a proper FD approximation to the boundary conditions.

An attempt to incorporate boundary conditions into a displacement FD scheme was made by Sochacki *et al.* (1991). They *a priori* assumed validity of the equation of motion at the discontinuity, wrote the equation in divergence form, and integrated it across the discontinuity. Then they approximated the integrated equation of motion.

Schoenberg and Muir (1989) developed calculus allowing one to replace a stack of thin flat anisotropic layers by an equivalent (in the long-wavelength limit) homogeneous anisotropic medium. In other words, they found Hooke's law for an averaged medium. They did this to simplify modeling of wave propagation for seismic exploration and, at the same time, to account for general anisotropy in sedimentary basins. Muir *et al.* (1992) applied the Schoenberg–Muir (1989) calculus to a grid cell that contains material discontinuity, that is, in general, they treated contents of the cell as a stack of thin flat layers that can be averaged by the Schoenberg–Muir calculus.

Zahradník and Priolo (1995) published a methodologically important work. They explicitly addressed the fundamental question of whether the heterogeneous approach is justified, namely, whether it is possible to find a heterogeneous formulation of the equation of motion. Assuming a discontinuity in material parameters they obtained from the equation of motion an expression whose dominant term is equivalent to the traction continuity condition. This result was interpreted as justification of the FD schemes constructed purely from equations of motion (without explicit treatment of the traction continuity).

Graves (1996) suggested an intuitive method how to determine effective material grid parameters in the 3D fourth-order velocity-stress staggered-grid schemes and numerically demonstrated good level of accuracy. Graves's (1996) article is important because, as far as we know, it was the first one on the staggered-grid modeling that explicitly and clearly explained how the heterogeneity is taken into account. Similarly clear explanation of the material grid parameterization was given by Ohminato and Chouet (1997) for their 3D second-order displacement-stress scheme.

Saenger *et al.* (2000) suggested to use for complex media a FD scheme on a partly staggered grid in which all stress-tensor components are located at the center of a grid cell and all displacement/velocity vector components are located at each corner of the cell.

In this article we first investigate a 1D problem in a medium consisting of two half-spaces. We consider boundary conditions at a welded planar interface of two half-spaces. We show simple physical models of the contact of two media and find an averaged medium representing the contact. We conclude the 1D case with a heterogeneous formulation of the equation of motion and Hooke's law, and the corresponding heterogeneous FD scheme.

We continue with investigation of a 3D problem. First we consider vectors of stress- and strain-tensor components and the elasticity matrix and then Hooke's law for an averaged medium representing (1) a planar-interface contact of two isotropic media and (2) a nonplanar-interface contact of two isotropic media. Because in the latter case 21 elastic coefficients are necessary to describe the averaged medium (while only two coefficients are necessary to describe any of the two media) we consider simplified boundary conditions for which the averaged medium can be described by only two elastic coefficients. Then we develop a heterogeneous FD scheme based on the simplified boundary conditions.

A series of numerical tests is presented to demonstrate very good accuracy of the developed FD scheme.

1D Case

A problem with both the 1D model and 1D wave propagation is a good example to explain the basics of our approach though, obviously, it cannot account for a general 3D case, which will be analyzed in the next section.

Equation of Motion

Consider perfectly elastic isotropic medium with density ρ and Lamé's elastic coefficients μ and λ being continuous functions of x. Then a plane wave propagation in the x direction is described by the equation of motion

$$\rho \ddot{d} = \tau_{,x} + f \tag{1a}$$

and Hooke's law

$$\tau = c\, d_{,x} \tag{1b}$$

where either $d(x, t)$ is the x component of the displacement $\vec{u}(d, 0, 0)$, $\tau(x, t)$ is the xx component of the stress tensor, $f(x, t)$ is the x component of the body force $\vec{f}(f, 0, 0)$, and $c(x) = \lambda(x) + 2\mu(x)$ in the case of P wave, or $d(x, t)$ is the y component of the displacement $\vec{u}(0, d, 0)$, $\tau(x, t)$ is the xy component of the stress tensor, $f(x, t)$ is the y component of the body force $\vec{f}(0, f, 0)$, and $c(x) = \mu(x)$ in the case of the *SH* wave (because the coordinate system can always be rotated so that the *S* wave could be the *SH* wave). The subscript x in $\tau_{,x}$ and $d_{,x}$ means the spatial derivative.

Equations (1a) and (1b) can be solved by the FD method. Let h and Δt be the grid spacing and time step. Let D_I^m, T_I^m, and F_I^m be the discrete approximations to $d_I^m = d(\mathrm{I}h, m\Delta t)$, $\tau_I^m = \tau(\mathrm{I}h, m\Delta t)$ and $f_I^m = f(\mathrm{I}h, m\Delta t)$. Then,

for example, the second-order displacement-stress FD scheme on a staggered grid is:

$$\frac{1}{(\Delta t)^2}\,(D_I^{m+1} - 2D_I^m + D_I^{m-1}) = \frac{1}{R_I}\frac{1}{h}\left(T_{I+1/2}^m - T_{I-1/2}^m\right), \tag{2a}$$

$$T_{I+1/2}^m = C_{I+1/2}\,\frac{1}{h}\,(D_{I+1}^m - D_I^m). \tag{2b}$$

R_I and C_I stand for some proper discrete approximations to density ρ and modulus c, respectively. If the medium is sufficiently smooth local values yield sufficiently accurate results. If equations (1a) and (1b) are modified to the velocity–stress formulation

$$\rho\dot{v} = \tau_{,x} + f \tag{3a}$$

$$\dot{\tau} = c\ v_{,x}, \tag{3b}$$

where $v = \dot{d}$, the FD scheme is

$$\frac{1}{\Delta t}\left(V_I^{m+1/2} - V_I^{m-1/2}\right) = \frac{1}{R_I}\frac{1}{h}\left(T_{I+1/2}^m - T_{I-1/2}^m\right) \tag{4a}$$

and

$$\frac{1}{\Delta t}\left(T_{I+1/2}^m - T_{I+1/2}^{m-1}\right) = C_{I+1/2}\,\frac{1}{h}\left(V_{I+1}^{m-1/2} - V_I^{m-1/2}\right), \tag{4b}$$

with V_I^m being the discrete approximation to $v_I^m = v(Ih,\ m\Delta t)$. Let us note that the fourth-order (in space) version of the scheme replaces the second-order approximations to the spatial derivatives on the right-hand sides of equations (4a) and (4b) by the fourth-order approximations.

Contact of Two Media

Consider now two perfectly elastic half-spaces with a welded interface in the plane $x = 0$. The wave propagation in the half-space is described by equations (1a) and (1b) with density ρ_1 and modulus c_1 in one half-space and ρ_2 and c_2 in the other half-space. At the welded interface the continuity of displacement and traction apply:

$$d_1\ (0) = d_2\ (0) \tag{5a}$$

and

$$\tau_1\ (0) = \tau_2\ (0). \tag{5b}$$

There are two usual approaches to solve the above problem by the FD method. The first one assumes the use of one of the above FD schemes for interior grid points in both half-spaces and a FD approximation to the boundary conditions (5a) and (5b) for grid points at the interface. The second approach uses one (the so-called heterogeneous) FD scheme (equations 2a, 2b, or 4a, 4b) for all grid points regardless of their positions with respect to the interface. The presence of the interface is taken into account by values of the discrete approximations to material parameters, namely, R_I and C_I.

Although the first approach is reasonable for simple geometry of the material discontinuity, it is hardly applicable with sufficient efficiency in case of complex discontinuities in 3D modeling. Having in mind mainly the 3D modeling it is crucial to find out how to determine grid values R_I and C_I in the heterogeneous-scheme approach.

Simple Physical Model

Let us consider a simple physical model of the contact of two elastic media in our 1D problem. Behavior of a linear elastic body can be represented by behavior of a spring. The strain e of the spring is proportional to the applied stress τ and inversely proportional to the elastic modulus c:

$$e = \frac{\tau}{c}. \tag{6}$$

A welded contact of two elastic bodies can be represented by a system of two springs connected in series (Fig. 1). The stresses acting on the springs are equal,

$$\tau_1 = \tau_2 = \tau, \tag{7}$$

in agreement with the traction-continuity condition. The strain e_1 of the first spring differs from the strain e_2 of the other spring (which also is in agreement with the conditions at the contact), and the resultant (total) strain e is

$$e = e_1 + e_2. \tag{8}$$

In a heterogeneous FD scheme we may have a grid point located at an interface. Such a grid point has to represent properly the welded contact. Therefore, we have to find average values of density and elastic modulus for the grid point at the interface such that the use of the average values in equations (1a) and (1b) would ensure the boundary conditions at the interface.

$$c_1 \neq c_2 \quad ; \quad \tau_1 = c_1 e_1 \quad , \quad \tau_2 = c_2 e_2$$

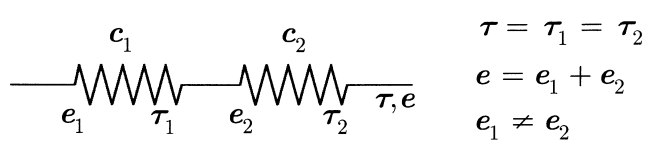

Figure 1. Connection of two elastic springs in series as a simple physical model of the contact of two elastic media in the considered 1D problem. c, elastic modulus; e, strain; τ, stress.

Going back to our physical model, we have to find an average elastic modulus $\bar{c}$ and average strain $\bar{e}$ such that the two connected identical springs with the same elastic moduli $\bar{c}$ and the same strains $\bar{e}$ is an equivalent system to the considered system of two springs with moduli c_1 and c_2 connected in series. Because the resultant strain e of the system of two identical springs connected in series is $e = 2\bar{e}$, the application of relations (6) and (7) to equation (8) gives

$$2\bar{e} = \frac{\tau}{c_1} + \frac{\tau}{c_2}$$

from which easily follows

$$\bar{e} = \frac{\tau}{\bar{c}} \tag{9}$$

where

$$\bar{e} = \frac{1}{2}(e_1 + e_2) \tag{10}$$

and

$$\bar{c} = \frac{2}{\frac{1}{c_1} + \frac{1}{c_2}} = \frac{2c_1c_2}{c_1 + c_2}. \tag{11}$$

Relations (9)–(11) show that the system of two springs (one with modulus c_1, the other with modulus c_2) connected in series can be equivalently replaced by the system of two identical springs, connected in series, with moduli $\bar{c}$ equal to the harmonic average of moduli c_1 and c_2 (equation 11) and strains $\bar{e}$ equal to the arithmetic average of strains e_1 and e_2 (equation 10).

In the elastodynamic problem we also have to include the acceleration. Consider a system of two connected particles with masses m_1 and m_2. The particles move together, that is, they have the same acceleration (which is in agreement with the displacement continuity at the welded contact of two media)

$$\vec{a}_1 = \vec{a}_2 = \vec{a}.$$

The forces acting on the particles are

$$\vec{F}_1 = m_1\vec{a} \text{ and } \vec{F}_2 = m_2\vec{a}. \tag{12}$$

The resultant force $\vec{F}$ acting on the system is

$$\vec{F} = \vec{F}_1 + \vec{F}_2. \tag{13}$$

The problem is to find an average mass $\bar{m}$ and average force $\vec{\bar{F}}$ such that the system of two connected particles of the same mass $\bar{m}$ and subject to the same forces $\vec{\bar{F}}$ be an equivalent system to the considered system of two particles of masses m_1 and m_2. The resultant force $\vec{F}$ of the equivalent system is

$$\vec{F} = 2\vec{\bar{F}}.$$

Using relations (12) and (13), we see that

$$2\vec{\bar{F}} = m_1\vec{a} + m_2\vec{a}$$

from which immediately follows

$$\vec{\bar{F}} = \bar{m}\vec{a} \tag{14}$$

where

$$\vec{\bar{F}} = \frac{1}{2}(\vec{F}_1 + \vec{F}_2) \tag{15}$$

and

$$\bar{m} = \frac{1}{2}(m_1 + m_2). \tag{16}$$

Thus, the condition of the same acceleration of two connected particles with masses m_1 and m_2 implies that the equivalent system of two particles consists of two connected particles with the same mass $\bar{m}$ equal to the arithmetic average of masses m_1 and m_2.

We can apply this result to unit volumes of a continuum. Denoting the densities of two media by ρ_1, and ρ_2 and acceleration by $\ddot{\vec{a}}$, equations (14) and (15) imply

$$\vec{\bar{F}} = \bar{\rho}\ddot{\vec{a}} \tag{17}$$

and

$$\bar{\rho} = \frac{1}{2}(\rho_1 + \rho_2). \tag{18}$$

Before we continue with the heterogeneous formulation of the equation of motion, let us mention that an alternative system of two springs connected in parallel is an appropriate model of the contact of two media in case when strains e_1 and e_2 are equal (strain-continuity condition at the contact) and stress τ_1 differs from stress τ_2 (discontinuity of stress at the contact). Such a situation corresponds to tangential deformation of the welded contact.

Both above considerations on the physical models can be mathematically unified. Let $\varphi_i(x)$, $c_i(x)$, and $g_i(x)$; $i \in \{1, 2\}$ be real functions of a real argument x such that

$$\begin{aligned} \varphi_1(x) &= c_1(x)\, g_1(x) \\ \varphi_2(x) &= c_2(x)\, g_2(x) \end{aligned} \tag{19}$$

and

$$\varphi_1(0) = \varphi_2(0). \tag{20}$$

Functions c_i and g_i may have discontinuities of the first order at $x = 0$. Define

$$\bar{g}\ (0)\ =\ \frac{1}{2}\ [g_1\ (0)\ +\ g_2\ (0)]. \tag{21}$$

Then it is easy to show that

$$\varphi_1\ (0)\ =\ \varphi_2\ (0)\ =\ \bar{c}\ (0)\ \bar{g}\ (0) \tag{22}$$

where

$$\bar{c}\ (0)\ =\ \frac{2}{\dfrac{1}{c_1\ (0)}\ +\ \dfrac{1}{c_2\ (0)}}\ =\ \frac{2\ c_1\ (0)\ c_2\ (0)}{c_1\ (0)\ +\ c_2\ (0)}. \tag{23}$$

If

$$c_1\ (x)\ =\ \frac{1}{r_1\ (x)}\ \text{and}\ c_2\ (x)\ =\ \frac{1}{r_2\ (x)}, \tag{24}$$

we have

$$\varphi_1\ (0)\ =\ \varphi_2\ (0)\ =\ \frac{1}{\bar{r}\ (0)}\ \bar{g}\ (0), \tag{25}$$

where

$$\bar{r}\ (0)\ =\ \frac{1}{2}\ [r_1\ (0)\ +\ r_2\ (0)]. \tag{26}$$

Heterogeneous Formulation of the Equation of Motion

Return now to our 1D problem in two elastic half-spaces with a welded interface in the plane $x = 0$. Equations (1a) and (1b) imply that the wave propagation in the half-spaces is described by equations

$$\ddot{d}_1\ =\ \frac{1}{\rho_1}\ (\tau_1,_x\ +\ f_1),\ \tau_1\ =\ c_1 d_1,_x \tag{27}$$

and

$$\ddot{d}_2\ =\ \frac{1}{\rho_2}\ (\tau_2,_x\ +\ f_2),\ \tau_2\ =\ c_2 d_2,_x. \tag{28}$$

The boundary conditions at the interface are

$$\ddot{d}_1(0)\ =\ \ddot{d}_2(0),\ \tau_1(0)\ =\ \tau_2(0). \tag{29}$$

Then it follows from the above analysis and equations (19)–(26) for the acceleration $\ddot{d}$ (0) and stress τ (0) at the interface that

$$\ddot{d}(0)\ =\ \frac{1}{\bar{\rho}(0)}\ [\overline{\tau,_x}(0)\ +\ \bar{f}(0)] \tag{30}$$

$$\tau(0)\ =\ \bar{c}(0)\ \overline{d,_x}(0) \tag{31}$$

where

$$\bar{\rho}(0)\ =\ \frac{1}{2}\ [\rho_1(0)\ +\ \rho_2(0)] \tag{32}$$

$$\bar{c}(0)\ =\ \frac{2}{\dfrac{1}{c_1(0)}\ +\ \dfrac{1}{c_2(0)}} \tag{33}$$

and

$$\overline{\tau,_x}(0)\ +\ \bar{f}(0)\ =\ \frac{1}{2}\ [\tau_1,_x(0)\ +\ \tau_2,_x(0)\ +\ f_1(0)\ +\ f_2(0)] \tag{34}$$

$$\overline{d,_x}(0)\ =\ \frac{1}{2}\ [d_1,_x(0)\ +\ d_2,_x(0)]. \tag{35}$$

Equations (30) and (31) are equations of motion and Hooke's law, respectively, applied to the interface. The harmonic average of elastic coefficients (equation 33), arithmetic average of densities (equation 32), and arithmetic averages of $\tau,_x + f$ (equation 34) and $d,_x$ (equation 35) ensure the displacement- and traction-continuity conditions at the interface.

Let us stress that we have now the same equations of motion for the interiors of the half-spaces and for the interface. The equations can be used without explicitly specifying boundary conditions if displacement, stress, density, and modulus are properly treated at the interface. In other words, we have found the heterogeneous formulation of the equations of motion for the considered 1D problem.

Heterogeneous Finite-Difference Scheme

In principle, we can solve the differential problem formulated by equations (1a), (1b), and (30)–(31) by a variety of FD approximations that would differ by accuracy and computational efficiency.

As stated before, it is desirable to have one FD scheme for all interior grid points regardless of their positions with respect to the material discontinuity and regardless of a gradient in material parameters.

Consider equation (1a)

$$\rho(x)\ \ddot{d}\ (x,t)\ =\ \tau,_x\ (x,t)\ +\ f\ (x,t)$$

and a staggered grid with positions for d and f shifted by half grid spacing, $h/2$, from positions for τ. Consider further a material discontinuity in either of three positions as shown in Figure 2. Density ρ as well as derivative of the stress $\tau,_x$ are discontinuous across the material discontinuity while displacement d (and consequently acceleration $\ddot{d}$) as well as stress τ are continuous across the material discontinuity.

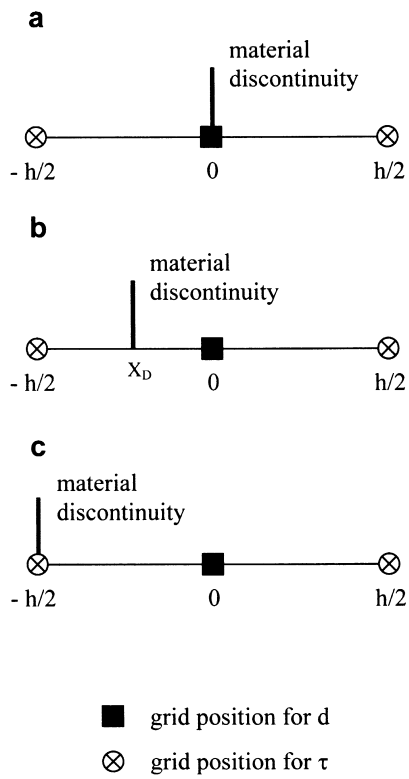

Figure 2. Three positions of a material discontinuity with respect to the spatial grid. Density ρ and the spatial derivative of stress, $\tau_{,x}$, are discontinuous across the material discontinuity while $\ddot{d}$ is continuous across it.

Assume first that the material discontinuity is located at $x = 0$, that is, at the position of d (Fig. 2a). Integrate the above equation (omitting, for simplicity, $f(x, t)$ which is continuous across the material discontinuity) over the grid spacing

$$\int_{-h/2}^{h/2} \rho\, \ddot{d}\, \mathrm{d}x = \int_{-h/2}^{h/2} \tau_{,x}\, \mathrm{d}x$$

$$\int_{-h/2}^{h/2} \rho\, \ddot{d}\, \mathrm{d}x = \lim_{\varepsilon^- \to 0^-} \int_{-h/2}^{\varepsilon^-} \tau_{,x}\, \mathrm{d}x + \lim_{\varepsilon^+ \to 0^+} \int_{\varepsilon^+}^{h/2} \tau_{,x}\, \mathrm{d}x.$$

Applying the mean value theorems to the above equation we get

$$\ddot{d}(x_1) \int_{-h/2}^{h/2} \rho\, \mathrm{d}x = \lim_{\varepsilon^- \to 0^-} \tau_{,x}(x_2) \int_{-h/2}^{\varepsilon^-} \mathrm{d}x + \lim_{\varepsilon^+ \to 0^+} \tau_{,x}(x_3) \int_{\varepsilon^+}^{h/2} \mathrm{d}x,$$

where $-h/2 < x_1 < h/2$, $-h/2 < x_2 < \varepsilon^-$; $\varepsilon^- \to 0^-$, and $\varepsilon^+ < x_3 < h/2$; $\varepsilon^+ \to 0^+$. The right-hand side of the previous equation gives

$$\tau_{,x}(x_2) \int_{-h/2}^{0} \mathrm{d}x + \tau_{,x}(x_3) \int_{0}^{h/2} \mathrm{d}x.$$

Given the spatial grid it is desirable to approximate $\ddot{d}(x_1)$ by $\ddot{d}(0)$, as well as both $\tau_{,x}(x_2)$ and $\tau_{,x}(x_3)$ by $\frac{1}{2}[\tau_{,x}(0^-) + \tau_{,x}(0^+)]$. Then the previous equation gives

$$\ddot{d}(0) \int_{-h/2}^{h/2} \rho\, \mathrm{d}x \doteq \frac{1}{2}\,[\tau_{,x}(0^-) + \tau_{,x}(0^+)] \int_{-h/2}^{h/2} \mathrm{d}x.$$

Define the integral arithmetic average of density

$$\bar{\rho} = \frac{1}{h} \int_{-h/2}^{h/2} \rho(x)\, \mathrm{d}x. \tag{36}$$

Then the above equation gives (including the body force f)

$$\bar{\rho}\ddot{d}(0) \doteq \frac{1}{2}\,[\tau_{,x}(0^-) + \tau_{,x}(0^+)] + f(0). \tag{37}$$

Assume that the material discontinuity is located at $x_D \neq 0$; $-h/2 < x_D < h/2$, see Figure 2b. The integration of equation (1a) leads to

$$\ddot{d}(x_1) \int_{-h/2}^{h/2} \rho\, \mathrm{d}x = \lim_{\varepsilon^- \to x_D^-} \tau_{,x}(x_2) \int_{-h/2}^{\varepsilon-} \mathrm{d}x + \lim_{\varepsilon^+ \to x_D^+} \tau_{,x}(x_3) \int_{\varepsilon+}^{h/2} \mathrm{d}x,$$

where $-h/2 < x_1 < h/2$, $-h/2 < x_2 < \varepsilon^-$; $\varepsilon^- \to x_D^-$, and $\varepsilon^+ < x_3 < h/2$; $\varepsilon^+ \to x_D^+$. The right-hand side of the above equation gives

$$\tau_{,x}(x_2) \int_{-h/2}^{x_D} \mathrm{d}x + \tau_{,x}(x_3) \int_{x_D}^{h/2} \mathrm{d}x.$$

As in the previous case, given the spatial grid, it is desirable to approximate $\ddot{d}(x_1)$ by $\ddot{d}(0)$. Both $\tau_{,x}(x_2)$ and $\tau_{,x}(x_3)$ can be approximated by $\tau_{,x}(0)$ because $\tau_{,x}$ is continuous at $x = 0$. Then we get

$$\bar{\rho}\ddot{d}(0) \doteq \tau_{,x}(0) + f(0). \tag{38}$$

Assuming the material discontinuity located at $x = -h/2$, see Figure 2c, we get again equation (38).

We have two equations, (37) and (38), in which spatial derivatives of the stress are to be replaced by appropriate FD approximations. If, however, we want only one FD scheme for all interior grid points, no matter what their positions are with respect to the material discontinuity, we formally replace $\frac{1}{2}[\tau_{,x}(0^-) + \tau_{,x}(0^+)]$ by $\tau_{,x}(0)$ in equation (37) and use only one equation, equation (38), as the basis for the FD

scheme. Thus we obviously introduce additional inaccuracy into the scheme if the material discontinuity is located in the grid position of displacement d.

Using our adopted grid indexing equation (38) gives

$$\rho_I^A \ddot{d}(x_I,t) \doteq \tau_{,x}(x_I,t) + f(x_I,t) \tag{39}$$

with

$$\rho_I^A = \frac{1}{h} \int_{x_{I-1/2}}^{x_{I+1/2}} \rho(x)\, \mathrm{d}x. \tag{40}$$

Thus, we can use the FD scheme (equations 2 or 4) with $R_I = \rho_I^A$.

Consider now equation (1b) divided by coefficient c

$$\frac{\tau(x,t)}{c(x)} = d_{,x}(x,\ t) \tag{41}$$

and a material discontinuity in either of three positions shown in Figure 3. The modulus c as well as the derivative of the displacement $d_{,x}$ are discontinuous across the material discontinuity, whereas displacement d as well as stress τ are continuous across the material discontinuity. The integration of equation (41) from $-h/2$ to $h/2$, similar to that of equation (1a), for the case shown in Figure 3a leads to

$$\tau(0) \doteq \bar{c}\, \frac{1}{2}\, [d_{,x}\,(0^-) + d_{,x}(0^+)] \tag{42}$$

with

$$\bar{c} = \left[\frac{1}{h} \int_{-h/2}^{h/2} \frac{\mathrm{d}x}{c(x)} \right]^{-1}. \tag{43}$$

The integration of terms in equation (41) for the cases shown in Figure 3b and 3c lead to

$$\tau(0) \doteq \bar{c}\, d_{,x}\,(0) \tag{44}$$

with $\bar{c}$ given by equation (43). Equations (42) and (44) are analogous to equations (37) and (38). Similarly, as we concluded discussion of the two latter equations with equation (39), we conclude here with

$$\tau(x_{I+1/2},\ t) \doteq c_{I+1/2}^H\, d_{,x}(x_{I+1/2},\ t) \tag{45}$$

where

$$c_{I+1/2}^H = \left[\frac{1}{h} \int_{x_I}^{x_{I+1}} \frac{\mathrm{d}x}{c(x)} \right]^{-1}. \tag{46}$$

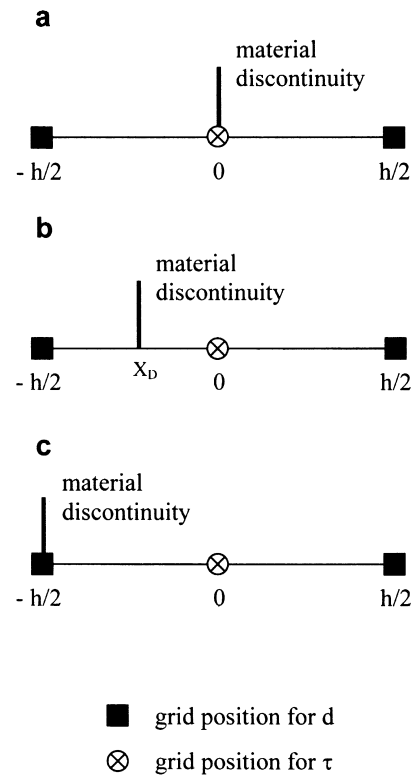

Figure 3. Three positions of a material discontinuity with respect to the spatial grid. Modulus c and the spatial derivative of displacement, $d_{,x}$, are discontinuous across the material discontinuity while stress τ is continuous across the material discontinuity.

Thus, we can use the FD scheme (equations 2 or 4) with $C_{I+1/2} = c_{I+1/2}^H$.

We note that the integration

$$\int_{x_I}^{x_{I+1}} \frac{\phi}{c(x)}\, \mathrm{d}x$$

leading to the integral harmonic averaging of a coefficient $c(x)$ was originally suggested by Tikhonov and Samarskii (see, e.g., Boore, 1972; Mitchell, 1969, p. 23) as a mathematical tool to avoid approximation of the derivative of the coefficient $c(x)$ in the FD approximation of terms

$$\frac{\partial}{\partial x}\left(c(x)\, \frac{\partial \psi}{\partial x} \right)$$

that appear in the displacement formulation of the equation of motion. The above integration is introduced by defining an auxiliary function ϕ as

$$\phi = c(x)\, \frac{\partial \psi}{\partial x}.$$

3D Case

Equation of Motion and Hooke's Law

Let density ρ, and elastic moduli λ and μ be functions of spatial coordinates x,y,z. Let displacement vector $\vec{u}(u, v, w)$, stress tensor τ_{ij}; $i, j \in \{x,y,z\}$, strain tensor ε_{ij}; $i,j \in \{x,y,z\}$, and body force per unit volume $\vec{f}(f_x, f_y, f_z)$ be functions of x,y,z and time t. The equation of motion for a perfectly elastic isotropic medium may be written as

$$\begin{aligned} \rho\ddot{u} &= \tau_{xx,x} + \tau_{yx,y} + \tau_{zx,z} + f_x \\ \rho\ddot{v} &= \tau_{xy,x} + \tau_{yy,y} + \tau_{zy,z} + f_y \\ \rho\ddot{w} &= \tau_{xz,x} + \tau_{yz,y} + \tau_{zz,z} + f_z, \end{aligned} \tag{47}$$

where $\ddot{u} = \partial^2 u/\partial t^2$, $\tau_{xx,x} = \partial\tau_{xx}/\partial x$, etc. Define vectors $\vec{\tau}$ and $\vec{\varepsilon}$, and elasticity matrix $\mathbf{E}$:

$$\vec{\tau} = [\tau_{xx}, \tau_{yy}, \tau_{zz}, \tau_{xy}, \tau_{yz}, \tau_{zx}]^T, \tag{48}$$

$$\vec{\varepsilon} = [\varepsilon_{xx}, \varepsilon_{yy}, \varepsilon_{zz}, \varepsilon_{xy}, \varepsilon_{yz}, \varepsilon_{zx}]^T, \tag{49}$$

and

$$\mathbf{E} = \begin{bmatrix} \lambda + 2\mu & \lambda & \lambda & 0 & 0 & 0 \\ \lambda & \lambda + 2\mu & \lambda & 0 & 0 & 0 \\ \lambda & \lambda & \lambda + 2\mu & 0 & 0 & 0 \\ 0 & 0 & 0 & 2\mu & 0 & 0 \\ 0 & 0 & 0 & 0 & 2\mu & 0 \\ 0 & 0 & 0 & 0 & 0 & 2\mu \end{bmatrix} \tag{50}$$

Hooke's law may be written as

$$\vec{\tau} = \mathbf{E}\,\vec{\varepsilon}. \tag{51}$$

Let us point out that in the isotropic heterogeneous medium each point of the medium is assigned two independent elastic coefficients plus density.

Boundary Conditions and Hooke's Law for an Averaged Medium

Let density ρ, and moduli λ and μ have a discontinuity of the first order across a surface S with normal vector $\vec{n}$. In other words, assume a material discontinuity on S. Then the welded-interface boundary conditions require continuity of displacement $\vec{u}\,(\vec{\xi})$ and traction $T(\vec{\xi},\vec{n})$ across the interface:

$$\vec{u}^+\,(\vec{\xi}) = \vec{u}^-\,(\vec{\xi}) \tag{52}$$

$$\vec{T}^+\,(\vec{\xi},\vec{n}) = \vec{T}^-\,(\vec{\xi},\vec{n}). \tag{53}$$

For simplicity, consider first a planar interface parallel to the xy-coordinate plane with a normal vector $\vec{n} = (0,0,1)$. Then the conditions (52) and (53) imply

$$\tau_{zx}^+ = \tau_{zx}^-, \quad \tau_{zy}^+ = \tau_{zy}^-, \quad \tau_{zz}^+ = \tau_{zz}^- \tag{54}$$

and

$$\varepsilon_{xx}^+ = \varepsilon_{xx}^-, \quad \varepsilon_{yy}^+ = \varepsilon_{yy}^-, \quad \varepsilon_{xy}^+ = \varepsilon_{xy}^-, \tag{55}$$

while τ_{xx}, τ_{yy}, τ_{xy}, ε_{zx}, ε_{zy}, and ε_{zz} may be discontinuous across the material discontinuity.

Given the continuous and discontinuous stress- and strain-tensor components, define

$$\vec{\tau}_C = [\tau_{zx}, \tau_{zy}, \tau_{zz}]^T \tag{56a}$$

$$\vec{\tau}_D = [\tau_{xx}, \tau_{yy}, \tau_{xy}]^T \tag{56b}$$

$$\vec{\varepsilon}_C = [\varepsilon_{xx}, \varepsilon_{yy}, \varepsilon_{xy}]^T \tag{57a}$$

$$\vec{\varepsilon}_D = [\varepsilon_{zx}, \varepsilon_{zy}, \varepsilon_{zz}]^T. \tag{57b}$$

Then

$$\vec{\tau}_C = \mathbf{R}\,\vec{\varepsilon}_D + \mathbf{P}\,\vec{\varepsilon}_C \tag{58a}$$

$$\vec{\tau}_D = \mathbf{P}^T\,\vec{\varepsilon}_D + \mathbf{S}\,\vec{\varepsilon}_C \tag{58b}$$

where

$$\mathbf{P} = \begin{bmatrix} 0 & 0 & 0 \\ 0 & 0 & 0 \\ \lambda & \lambda & 0 \end{bmatrix} \tag{59a}$$

$$\mathbf{R} = \begin{bmatrix} 2\mu & 0 & 0 \\ 0 & 2\mu & 0 \\ 0 & 0 & \lambda + 2\mu \end{bmatrix} \tag{59b}$$

$$\mathbf{S} = \begin{bmatrix} \lambda + 2\mu & \lambda & 0 \\ \lambda & \lambda + 2\mu & 0 \\ 0 & 0 & 2\mu \end{bmatrix}. \tag{59c}$$

Redefining vectors $\vec{\tau}$ and $\vec{\varepsilon}$, and matrix $\mathbf{E}$,

$$\vec{\tau} = \begin{bmatrix} \vec{\tau}_C \\ \vec{\tau}_D \end{bmatrix}, \quad \vec{\varepsilon} = \begin{bmatrix} \vec{\varepsilon}_D \\ \vec{\varepsilon}_C \end{bmatrix}, \tag{60a}$$

$$\mathbf{E} = \begin{bmatrix} \mathbf{R} & \mathbf{P} \\ \mathbf{P}^T & \mathbf{S} \end{bmatrix}, \tag{60b}$$

we can write Hooke's law for each of the two media in contact again in the form

$$\vec{\tau} = \mathbf{E}\,\vec{\varepsilon}. \tag{61}$$

What we want now is to find the same form of Hooke's law for an averaged medium that would represent the planar-interface contact of the two media.

From equation (58) we get

$$\vec{\varepsilon}_D = -\mathbf{R}^{-1}\mathbf{P}\,\vec{\varepsilon}_C + \mathbf{R}^{-1}\,\vec{\tau}_C \tag{62a}$$

$$\vec{\tau}_D = [\mathbf{S} - \mathbf{P}^T\mathbf{R}^{-1}\mathbf{P}]\,\vec{\varepsilon}_C + \mathbf{P}^T\mathbf{R}^{-1}\,\vec{\tau}_C \tag{62b}$$

Vectors $\vec{\varepsilon}_D$ and $\vec{\tau}_D$, as well as the matrices on the right-hand sides of equations (62), are discontinuous across the interface, whereas vectors $\vec{\varepsilon}_C$ and $\vec{\tau}_C$ are continuous. Let D be a discontinuous function across the interface, that is, $D^+ \neq D^-$. Define the averaged function D^A as

$$D^A = \frac{1}{2}(D^+ + D^-). \tag{63}$$

Then we get from equations (62) the averaged vectors $\vec{\varepsilon}_D^A$ and $\vec{\tau}_D^A$ as

$$\vec{\varepsilon}_D^A = (-\mathbf{R}^{-1}\mathbf{P})^A\vec{\varepsilon}_C + (\mathbf{R}^{-1})^A\vec{\tau}_C \tag{64a}$$

$$\vec{\tau}_D^A = (\mathbf{S} - \mathbf{P}^T\mathbf{R}^{-1}\mathbf{P})^A\vec{\varepsilon}_C + (\mathbf{P}^T\mathbf{R}^{-1})^A\vec{\tau}_C. \tag{64b}$$

Expressing $\vec{\tau}_C^A \equiv \vec{\tau}_C$ and $\vec{\tau}_D^A$ as functions of $\vec{\varepsilon}_C$ and $\vec{\varepsilon}_D^A$, we get a system of equations analogous to system (58):

$$\vec{\tau}_C^A \equiv \vec{\tau}_C = \tilde{\mathbf{R}}\,\vec{\varepsilon}_D^A + \tilde{\mathbf{P}}\,\vec{\varepsilon}_C \tag{65a}$$

$$\vec{\tau}_D^A = \tilde{\mathbf{P}}^T\,\vec{\varepsilon}_D^A + \tilde{\mathbf{S}}\,\vec{\varepsilon}_C \tag{65b}$$

and

$$\tilde{\mathbf{P}} = [(\mathbf{R}^{-1})^A]^{-1}\,(\mathbf{R}^{-1}\mathbf{P})^A \tag{66a}$$

$$\tilde{\mathbf{R}} = [(\mathbf{R}^{-1})^A]^{-1} \tag{66b}$$

$$\tilde{\mathbf{S}} = (\mathbf{S} - \mathbf{P}^T\mathbf{R}^{-1}\mathbf{P})^A + (\mathbf{P}^T\mathbf{R}^{-1})^A[(\mathbf{R}^{-1})^A]^{-1}\,(\mathbf{R}^{-1}\mathbf{P})^A. \tag{66c}$$

Defining vectors $\vec{\tau}^A$ and $\vec{\varepsilon}^A$, and matrix $\tilde{\mathbf{E}}$ in analogy with vectors $\vec{\tau}$ and $\vec{\varepsilon}$, and matrix $\mathbf{E}$ defined by equation (60), that is,

$$\vec{\tau}^A = \begin{bmatrix}\vec{\tau}_C^A\\ \vec{\tau}_D^A\end{bmatrix}, \quad \vec{\varepsilon}^A = \begin{bmatrix}\vec{\varepsilon}_D^A\\ \vec{\varepsilon}_C^A\end{bmatrix};$$
$$\vec{\tau}_C^A \equiv \vec{\tau}_C, \quad \vec{\varepsilon}_C^A \equiv \vec{\varepsilon}_C, \tag{67a}$$

and

$$\tilde{\mathbf{E}} = \begin{bmatrix}\tilde{\mathbf{R}} & \tilde{\mathbf{P}}\\ \tilde{\mathbf{P}}^T & \tilde{\mathbf{S}}\end{bmatrix} \tag{67b}$$

we get Hooke's law for the averaged medium (representing the planar-interface contact of the two media) in the same form as for each of the two media:

$$\vec{\tau}^A = \tilde{\mathbf{E}}\,\vec{\varepsilon}^A. \tag{68}$$

The substantial difference between laws (61) and (68) is that matrix $\tilde{\mathbf{E}}$ for the averaged medium has five independent nonzero elements and the averaged medium is transversely isotropic, whereas matrix $\mathbf{E}$ for any of the two isotropic media in contact has only two independent nonzero elements. In other words, an exact heterogeneous formulation of the elastodynamic equation for a medium having a planar material discontinuity parallel with a coordinate plane (i.e., perpendicular to a coordinate axis) substantially increases the number of elastic coefficients necessary to describe the medium. As a consequence, a corresponding FD scheme requires a substantially increased computer memory.

Have a quick look now at a planar material discontinuity in a general position in a Cartesian coordinate system. Let a normal vector be $\vec{n} = (n_x, n_y, n_z)$ with all nonzero elements. Then the procedure of finding Hooke's law for an averaged medium representing the planar-interface contact of two media may be as follows: Find a Cartesian coordinate system $x'y'z'$ in which $\vec{n}$ is parallel to the z' axis, that is, the interface is parallel to the $x'y'$-coordinate plane. Calculate matrices $\tilde{\mathbf{R}}'$, $\tilde{\mathbf{P}}'$, and $\tilde{\mathbf{S}}'$ (equations 66), and construct matrix $\tilde{\mathbf{E}}'$ (equations 67b). (Matrix $\tilde{\mathbf{E}}'$ has five independent nonzero elements.) Transform matrix $\tilde{\mathbf{E}}'$ into matrix $\tilde{\mathbf{E}}$ in the original coordinate system xyz. The symmetric matrix $\tilde{\mathbf{E}}$ has, in general, all elements nonzero. This means that all strain-tensor components are necessary to calculate each stress-tensor component at a point of the interface and 21 nonzero elastic coefficients are necessary at the point.

Consider now a general nonplanar smooth surface S being an interface between two media. At any point of the interface general surface S can be approximated by a planar surface tangential to surface S at the point. Then the aforementioned procedure of finding matrix $\tilde{\mathbf{E}}$ at the point can be applied. This means that 21 nonzero elastic coefficients are necessary at each point of the material discontinuity for heterogeneous formulation of the elastodynamic equation. Thinking of a corresponding FD scheme for a medium with material discontinuities, we have two possibilities: (1) To calculate 21 nonzero elastic coefficients for each grid point and store them in memory during the whole FD time-integration and (2): to store only 2 + 2 elastic coefficients and two angles (specifying orientation of an approximating tangential planar interface) for each grid point and calculate matrix $\tilde{\mathbf{E}}$ at each time step of the FD time-integration at each grid point.

It is obvious that while the first possibility requires tremendous computer memory, the second one substantially increases computational time. The previous analysis for the planar interface corresponds to the application of Schoenberg and Muir (1989) calculus applied to the special case of one interface between two homogeneous isotropic half-spaces.

Simplified Approach

Assume a discontinuity of material parameters across smooth surface S with normal vector $\vec{n}(x, y, z)$. Consider Hooke's law in the form

$$\begin{aligned}
\tau_{xx} &= \kappa\theta + \tfrac{2}{3}\mu(2u_{,x} - v_{,y} - w_{,z}) \\
\tau_{yy} &= \kappa\theta + \tfrac{2}{3}\mu(-u_{,x} + 2v_{,y} - w_{,z}) \\
\tau_{zz} &= \kappa\theta + \tfrac{2}{3}\mu(-u_{,x} - v_{,y} + 2w_{,z}) \\
\tau_{xy} &= \tau_{yx} = \mu(u_{,y} + v_{,x}) \\
\tau_{yz} &= \tau_{zy} = \mu\,(v_{,z} + w_{,y}) \\
\tau_{zx} &= \tau_{xz} = \mu\,(w_{,x} + u_{,z})
\end{aligned} \tag{69}$$

where θ is volume dilatation

$$\theta = u_{,x} + v_{,y} + w_{,z}$$

and κ is bulk modulus, $\kappa = \lambda + \frac{2}{3}\mu$.

Assume (1) continuity of a trace of the stress tensor, $\tau_{xx} + \tau_{yy} + \tau_{zz} = 3\kappa\theta$; (2) continuity of deviatoric parts of the normal stress-tensor components; and (3) continuity of shear stress-tensor components across the material discontinuity S.

Then the application of equations (19)–(23) to the (assumed) continuous quantities leads to harmonic averaging of κ, harmonic averaging of μ, and arithmetic averaging of spatial derivatives of the displacement component at the material discontinuity.

It is now clear that the previous assumptions on continuity simplify the problem of averaging because they imply that only two elastic parameters (harmonic averages of κ and μ) describe the averaged medium representing the contact of two media along surface S. In other words, in a corresponding FD scheme, the number of elastic parameters would be the same as that for a smoothly heterogeneous medium without material discontinuities. Obviously, the question is how accurate such a FD scheme is.

The equation of motion (52) for the u component of displacement can be written in the form

$$\ddot{u} = \frac{1}{\rho} F^u,$$

where $F^u = \tau_{xx,x} + \tau_{yx,y} + \tau_{zx,z} + f_x$. The particle acceleration $\ddot{u}$ has to be continuous across the material discontinuity because displacement is continuous. Application of equations (19)–(21) and (24)–(26) leads to arithmetic averaging of ρ and arithmetic averaging of F^u at the material discontinuity.

This is also true about the equations for the v and w components of displacement.

Heterogeneous Finite-Difference Scheme

Here we construct a FD scheme based on the previous simplified approach. In order to have one FD scheme for all interior grid points regardless of the presence and position of the material discontinuity or gradient in material parameters, we apply a similar approach to equations (47) and (69) as we applied to equations (1a) and (1b) in the 1D case. We cover a computational region by a staggered grid with a constant spatial grid spacing h in all three directions. We assume the spatial grid positions of discrete approximations to displacement and stress-tensor components, that is, U, V, W, and T^{xx}, T^{yy}, T^{zz}, T^{xy}, T^{yz}, T^{zx}, as it is shown in Figure 4.

Volume Arithmetic and Harmonic Averaging. Consider a grid cell $h \times h \times h$ with a center at $(x_I, y_{K+1/2}, z_{L+1/2})$ and define the volume integral

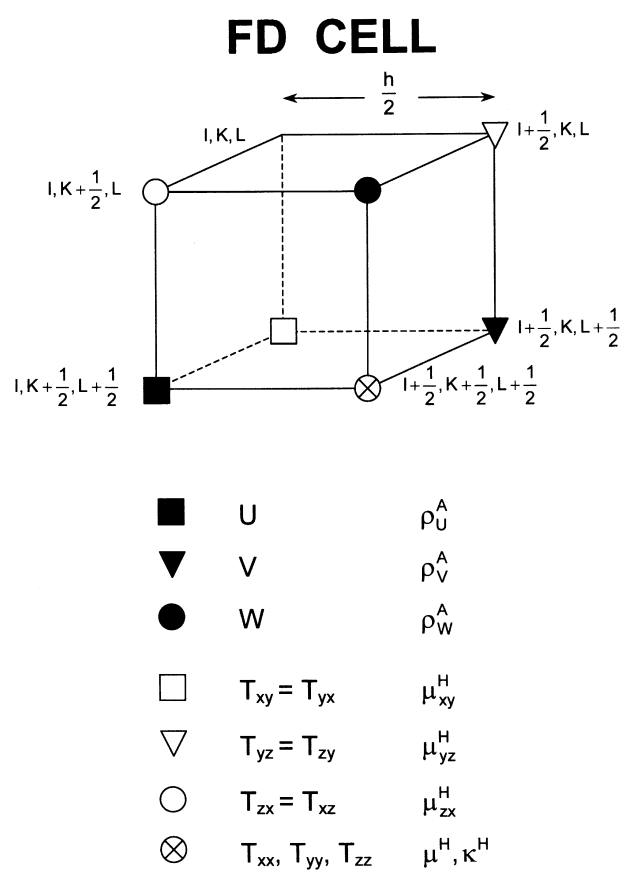

Figure 4. A FD grid cell with positions of the wave-field variables and effective media parameters.

$$\iiint_{V^u} \mathrm{d}V^u = \int_{x_{I-1/2}}^{x_{I+1/2}} \int_{y_K}^{y_{K+1}} \int_{z_L}^{z_{L+1}} \mathrm{d}x\ \mathrm{d}y\ \mathrm{d}z.$$

Analogously with the 1D case, the integration of equation (47) for the u component of displacement,

$$\iiint_{V^u} \rho\ddot{u}\ \mathrm{d}V^u = \iiint_{V^u} (\tau_{xx,x} + \tau_{yx,y} + \tau_{zx,z} + f_x)\ \mathrm{d}V^u \quad (70)$$

leads to the approximation

$$\begin{aligned}&\rho^A_{I,K+1/2,L+1/2}\ \ddot{u}(x_I,\ y_{K+1/2},\ z_{L+1/2},\ t) \doteq \\ &\tau_{xx,x}(x_I,\ y_{K+1/2},\ z_{L+1/2},\ t) + \tau_{yx,y}(x_I,\ y_{K+1/2},\ z_{L+1/2},\ t) \\ &+ \tau_{zx,z}(x_I,\ y_{K+1/2},\ z_{L+1/2},\ t) + f_x(x_I,\ y_{K+1/2},\ z_{L+1/2},\ t)\end{aligned} \quad (71)$$

where

$$\rho^A_{I,K+1/2,L+1/2} = \frac{1}{h^3} \iiint_{V^u} \rho\ \mathrm{d}V^u \quad (72)$$

is the volume arithmetic average of density.

Analogously, applying volume integrals

$$\iiint_{V^v} \mathrm{d}V^v = \int_{x_I}^{x_{I+1}} \int_{y_{K-1/2}}^{y_{K+1/2}} \int_{z_L}^{z_{L+1}} \mathrm{d}x\ \mathrm{d}y\ \mathrm{d}z$$

and

$$\iiint_{V^w} \mathrm{d}V^w = \int_{x_I}^{x_{I+1}} \int_{y_K}^{y_{K+1}} \int_{z_{L-1/2}}^{z_{L+1/2}} \mathrm{d}x\ \mathrm{d}y\ \mathrm{d}z$$

to equations (47) for the v and w components of displacement, respectively, we can obtain equations for $\ddot{v}(x_{I+1/2},\ y_K,\ z_{L+1/2},\ t)$ and $\ddot{w}(x_{I+1/2},\ y_{K+1/2},\ z_L,\ t)$.

Denote the isotropic and deviatoric parts of τ_{xx} by τ^I_{xx} and τ^D_{xx}, respectively.

Then

$$\tau_{xx} = \tau^I_{xx} + \tau^D_{xx} \quad (73)$$

and

$$\begin{aligned}\tau^I_{xx} &= \kappa\theta \\ \tau^D_{xx} &= \frac{2}{3}\mu(2u_{,x} - v_{,y} - w_{,z}).\end{aligned} \quad (74)$$

Consider a grid cell $h \times h \times h$ with a center at $(x_{I+1/2},\ y_{K+1/2},\ z_{L+1/2})$ and define the volume integral

$$\iiint_{V^{xx}} \mathrm{d}V^{xx} = \int_{x_I}^{x_{I+1}} \int_{y_K}^{y_{K+1}} \int_{z_L}^{z_{L+1}} \mathrm{d}x\ \mathrm{d}y\ \mathrm{d}z.$$

The integration of equation (74) divided by κ

$$\iiint_{V^{xx}} \frac{\tau^I_{xx}}{\kappa}\ \mathrm{d}V^{xx} = \iiint_{V^{xx}} \theta \mathrm{d}V^{xx}$$

leads to

$$\tau^I_{xx}\left(x_{I+1/2},\ y_{K+1/2},\ z_{L+1/2},\ t\right) \doteq \kappa^H_{I+1/2,\ K+1/2,\ L+1/2}\ \theta\left(x_{I+1/2},\ y_{K+1/2},\ z_{L+1/2},\ t\right), \quad (75)$$

where

$$\kappa^H_{I+1/2,\ K+1/2,\ L+1/2} = \left[\frac{1}{h^3} \iiint_{V^{xx}} \frac{\mathrm{d}V^{xx}}{\kappa}\right]^{-1}$$

is the volume harmonic average of bulk modulus.

Similarly, we can obtain

$$\begin{aligned}\tau^D_{xx}\left(x_{I+1/2},\ y_{K+1/2},\ z_{L+1/2},\ t\right) &\doteq \frac{2}{3}\mu^H_{I+1/2,K+1/2,L+1/2} \\ &\left[2u_{,x}\left(x_{I+1/2},\ y_{K+1/2},\ z_{L+1/2},\ t\right) - v_{,y}\left(x_{I+1/2},\ y_{K+1/2},\ z_{L+1/2},\ t\right)\right. \\ &\left. - w_{,z}\left(x_{I+1/2},\ y_{K+1/2},\ z_{L+1/2},\ t\right)\right]\end{aligned} \quad (76)$$

Substituting τ^I_{xx} from equation (75) and τ^D_{xx} from equation (76) into equation (73), we have

$$\tau_{xx}\left(x_{I+1/2},\ y_{K+1/2},\ z_{L+1/2},\ t\right) \doteq \kappa^H_{I+1/2,\ K+1/2,\ L+1/2}\ \theta + \frac{2}{3}\mu^H_{I+1/2,\ K+1/2,\ L+1/2}\ (2u_{,x} - v_{,y} - w_{,z}), \quad (77)$$

where θ, $u_{,x}$, $v_{,y}$, and $w_{,z}$ are values at $(x_{I+1/2},\ y_{K+1/2},\ z_{L+1/2},\ t)$. Analogously, we can obtain equations for $\tau_{yy}(x_{I+1/2},\ y_{K+1/2},\ z_{L+1/2},\ t)$ and $\tau_{zz}(x_{I+1/2},\ y_{K+1/2}, z_{L+1/2},\ t)$.

Finite-Difference scheme. Time and spatial derivatives in equation (47) may be approximated by standard second-order and fourth-order FD formulas, respectively. Applying them, we obtain

$$
\begin{aligned}
U^{m+1}_{I,K+1/2,L+1/2} &= 2U^{m}_{I,K+1/2,L+1/2} - U^{m-1}_{I,K+1/2,L+1/2} \\
&+ \frac{\Delta^2 t}{h}\frac{1}{\rho^A_{I,K+1/2,L+1/2}}\Bigg[a\left(T^{xx,m}_{I+3/2,K+1/2,L+1/2} - T^{xx,m}_{I-3/2,K+1/2,L+1/2}\right) \\
&+ b\left(T^{xx,m}_{I+1/2,K+1/2,L+1/2} - T^{xx,m}_{I-1/2,K+1/2,L+1/2}\right) \\
&+ a\left(T^{xy,m}_{I,K+2,L+1/2} - T^{xy,m}_{I,K-1,L+1/2}\right) \\
&+ b\left(T^{xy,m}_{I,K+1,L+1/2} - T^{xy,m}_{I,K,L+1/2}\right) \\
&+ a\left(T^{zx,m}_{I,K+1/2,L+2} - T^{zx,m}_{I,K+1/2,L-1}\right) \\
&+ b\left(T^{zx,m}_{I,K+1/2,L+1} - T^{zx,m}_{I,K+1/2,L}\right)\Bigg] \\
&+ \frac{\Delta^2 t}{\rho^A_{I,K+1/2,L+1/2}} F^{x,m}_{I,K+1/2,L+1/2} ,
\end{aligned}
$$

where m is the time index, $a = -1/24$, $b = 9/8$, and

$$
\rho^A_{I,K+1/2,L+1/2} = \frac{1}{h^3}\int_{x_{I-1/2}}^{x_{I+1/2}}\int_{y_K}^{y_{K+1}}\int_{z_L}^{z_{L+1}} \rho \, \mathrm{d}x \, \mathrm{d}y \, \mathrm{d}z .
$$

For equation (77), we obtain

$$
\begin{aligned}
T^{xx,m}_{I+1/2,K+1/2,L+1/2} &= \frac{1}{h}\Bigg\{\left(\kappa^H_{I+1/2,K+1/2,L+1/2} + \frac{4}{3}\mu^H_{I+1/2,K+1/2,L+1/2}\right) \\
&\quad \Big[a\left(U^m_{I+2,K+1/2,L+1/2} - U^m_{I-1,K+1/2,L+1/2}\right) \\
&\quad + b\left(U^m_{I+1,K+1/2,L+1/2} - U^m_{I,K+1/2,L+1/2}\right)\Big] \\
&\quad + \left(\kappa^H_{I+1/2,K+1/2,L+1/2} - \frac{2}{3}\mu^H_{I+1/2,K+1/2,L+1/2}\right) \\
&\quad \Big[a\left(V^m_{I+1/2,K+2,L+1/2} - V^m_{I+1/2,K-1,I+1/2}\right) \\
&\quad + b\left(V^m_{I+1/2,K+1,L+1/2} - V^m_{I+1/2,K,L+1/2}\right) \\
&\quad + a\left(W^m_{I+1/2,K+1/2,L+2} - W^m_{I+1/2,K+1/2,L-1}\right) \\
&\quad + b\left(W^m_{I+1/2,K+1/2,L+1} - W^m_{I+1/2,K+1/2,L}\right)\Big]\Bigg\} ,
\end{aligned}
$$

where

$$
\kappa^H_{I+1/2,K+1/2,L+1/2} = \left[\frac{1}{h^3}\int_{x_I}^{x_{I+1}}\int_{y_K}^{y_{K+1}}\int_{z_L}^{z_{L+1}} \frac{1}{\kappa} \, \mathrm{d}x \, \mathrm{d}y \, \mathrm{d}z\right]^{-1}
$$

and

$$
\mu^H_{I+1/2,K+1/2,L+1/2} = \left[\frac{1}{h^3}\left[\int_{x_I}^{x_{I+1}}\int_{y_K}^{y_{K+1}}\int_{z_L}^{z_{L+1}} \frac{1}{\mu} \, \mathrm{d}x \, \mathrm{d}y \, \mathrm{d}z\right]^{-1}.
$$

Analogously we obtain the FD approximations for the remaining displacement and stress-tensor components. They are given in the Appendix.

As already mentioned, we did not include the arithmetic averaging of the spatial derivatives of the displacement and stress-tensor components at the material discontinuity and thus introduced additional inaccuracy into the FD scheme if it is applied at the material discontinuity. We did this in order to have one simple scheme for all interior grid points.

We do not show here the velocity-stress scheme because it is very easy to obtain by simple modification of the displacement-stress scheme (as we illustrated in the 1D case).

Graves (1996) intuitively suggested averaging of material parameters that is relatively close to ours—see equations (9) in his article. In a special case of 2D model with a discontinuity separating two homogeneous blocks and coinciding with a grid plane going through positions of the shear stress-tensor components, his averaging of the shear modulus is the same as ours.

Free Surface. The free surface cannot be treated as an internal discontinuity since the displacement and traction continuity do not apply at the free surface. The techniques available for simulating the planar traction-free surface are presented and compared in the article by Kristek *et al.* (2002). In the numerical tests presented below we use the H-AFDA or W-AFDA techniques described by Kristek *et al.* (2002).

Nonreflecting Boundaries. In principle a variety of nonreflecting boundaries may be applied. In our numerical tests we used the combination of the first-order operator of Higdon (1991) with the A1 condition of Clayton and Engquist (1977) as suggested by P.-C. Liu and R. J. Archuleta (personal comm., 2000). The explicit formula is given in the Appendix.

Stability and Grid Dispersion. In an unbounded homogeneous medium, our FD scheme does not differ from the displacement-stress scheme presented by Moczo *et al.* (2000). The same is true about the velocity-stress scheme. The velocity-stress scheme with volume harmonic averaging of elastic moduli and volume arithmetic averaging of density does not differ in an unbounded homogeneous medium from that described by Graves (1996). Stability and grid dispersion for both schemes were analyzed in detail by Moczo *et al.* (2000). Stability and grid dispersion of the fourth-order staggered-grid FD schemes in the presence of a free surface or heterogeneity of the medium is much more difficult to analyze. Stability conditions and grid dispersion are therefore verified by numerical tests.

Computational Efficiency. Assume first that the elastic moduli κ and μ as well as density ρ can change between each two grid points. Then each grid position of displacement/particle velocity should be assigned its volume arithmetic average of density, say, ρ^A_U, ρ^A_V, and ρ^A_W. Similarly, each grid position of shear stress-tensor components should be assigned its volume harmonic average of μ, say μ^H_{XY}, μ^H_{YZ}, μ^H_{ZX}, and the grid position of the normal stress-tensor com-

ponents should be also assigned the volume harmonic averages of κ and μ, say κ^H and μ^H. Let p denote the number of bytes for the used real-value precision ($p = 4$ in single precision and $p = 8$ in double precision). Let *MX, MY*, and *MZ* be the numbers of grid cells in the *x, y*, and *z* directions, respectively. Then displacement components and material parameters that have to be stored as well as the number of bytes N^P_{DS} occupied by these quantities in the displacement-stress FD scheme are

$$U^m,\ V^m,\ W^m,\ U^{m-1},\ V^{m-1},\ W^{m-1}$$
$$\rho^A_U,\ \rho^A_V,\ \rho^A_W,\ \kappa^H,\ \mu^H,\ \mu^H_{XY},\ \mu^H_{YZ},\ \mu^H_{ZX}$$
$$N^P_{\mathrm{DS}} = p{\cdot}MX{\cdot}MY{\cdot}MZ{\cdot}14$$

Similarly, the particle-velocity and stress-tensor components, material parameters, and the number of bytes N^P_{VS} in the velocity-stress FD scheme are

$$\dot{U}^{m-1/2}, \dot{V}^{m-1/2}, \dot{W}^{m-1/2}, T^{m-1}_{XX}, T^{m-1}_{YY}, T^{m-1}_{ZZ}, T^{m-1}_{XY}, T^{m-1}_{YZ}, T^{m-1}_{ZX}$$
$$\rho^A_U,\ \rho^A_V,\ \rho^A_W,\ \kappa^H,\ \mu^H,\ \mu^H_{XY},\ \mu^H_{YZ},\ \mu^H_{ZX}$$
$$N^P_{\mathrm{VS}} = p{\cdot}MX{\cdot}MY{\cdot}MZ{\cdot}17$$

These memory requirements may be reduced by more than one order using the memory-optimization techniques described by Moczo *et al.* (1999, 2001).

Numerical Tests

We tested accuracy of our FD scheme by comparing the FD synthetics with those calculated using the discrete-wavenumber (DWN) method (Bouchon, 1981; computer code Axitra by Coutant, [1989]). Here we show results for 12 configurations in four types of models: a contact of two half-spaces, an interior layer between two half-spaces, a single layer over a half-space, and a moon valley.

Model of Two Half-Spaces

Two homogeneous half-spaces are separated by a horizontal planar interface located at $z = 0$. The parameters of the model are given in Table 1. A point double-couple source was located in the lower half-space and its Cartesian coordinates (*x,y,z*) were (0,0,1300) m. The source was simulated using a body-force term by a method suggested by Frankel (1993) and adapted for a staggered-grid by Graves (1996). Gabor signal, $s(t) = \exp\{-[\omega(t - t_s)/\gamma]^2\} \cos[\omega(t - t_s) + \theta]$, was used as a source time function. Here, $\omega = 2\pi f_p$, $t \in \langle 0, 2t_s \rangle$, f_p is the predominant frequency, γ controls the width of the signal, θ is a phase shift, and $t_s = 0.45\gamma/f_p$. The parameters of the source are given in Table 2. A receiver was located in the upper half-space and its coordinates were (1500, 0, −500) m.

One and the same physical model is calculated using two different grids (see the upper part of Fig. 5). A size of the grid spacing h in the first grid is determined as $h = \lambda_{\min}/6$, that is, the minimum wavelength $\lambda_{\min}$, which should be sufficiently accurately propagated in the grid, is six times larger than the grid spacing. This spatial sampling has been shown appropriate by the stability and grid-dispersion analysis in the homogeneous medium (Moczo *et al.*, 2000). The question is whether this spatial sampling is sufficient if there is a material discontinuity in the medium.

Table 1
Model Parameters: Model of Two Half-Spaces

	α (m/sec)	β (m/sec)	ρ (kg/m^3)
Upper half-space	2250	1250	1600
Lower half-space	5468	3126	1800

α, *P*-wave velocity; β, *S*-wave velocity; ρ, density.

Table 2
Source Parameters

M_0 (N m)	ϕ_S (deg)	δ (deg)	λ (deg)	γ	f_P	θ	t_S
10^{16}	0	45	90	1.5	0.225	π/2	3.0

M_0, scalar seismic moment; ϕ_S, strike; δ, dip; λ, rake; γ, f_P, θ, and t_S, parameters of Gabor signal.

Therefore, we calculated the same physical model also using three times finer grid with the spatial grid spacing $H = \lambda_{\min}/18$. The numbers of grid cells in the *x, y*, and *z* directions were $MX = 352$, $MY = 352$, and $MZ = 380$ in the $h \times h \times h$ grid and $MX = 520$, $MY = 520$, and $MZ = 670$ in the $H \times H \times H$ grid. The spatial grid spacings were $h = 200$ m and $H = 66.6$ m, time steps $\Delta t = 0.018$ sec and $\Delta t = 0.006$ sec, respectively. Moreover, we compared both calculations with an independent solution by the DWN method. Figure 5 shows the two FD and DWN synthetics (U component, velocity seismograms). The two FD solutions are within thickness of the line and are in a good agreement with the DWN solution. This result confirms that with our FD scheme, six grids spacing per minimum wavelength is sufficiently accurate spatial sampling even if there is a material discontinuity in the medium.

Interior Layer

Interface Parallel to a Grid Plane. A single horizontal homogeneous layer is located in between two different but identical homogeneous half-spaces. In order to test sensitivity of our scheme to different positions of the layer–half-space interface with respect to a spatial grid, we considered five different thicknesses of the layer using the same spatial grid (see the upper part of Fig. 6). A point double-couple source was located in the lower half-space. The parameters of the models are given in Table 3; parameters of the source, the same as in the case of two half-spaces, in Table 2.

A receiver was located inside the layer, 200 m above the lower layer–half-space interface. If coordinates of the source were (0, 0, 0) m, coordinates of the receiver were (1450, 0,

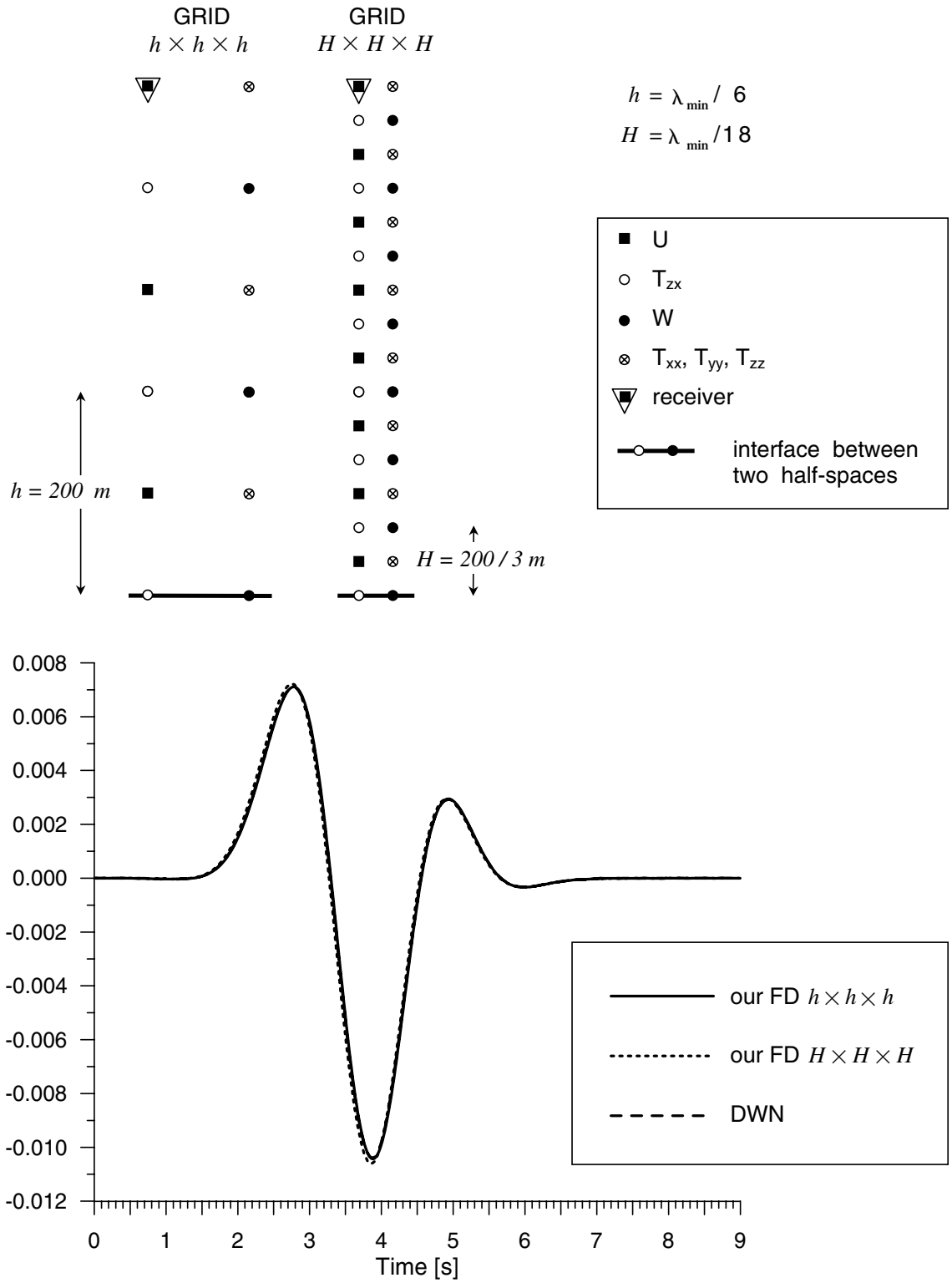

Figure 5. *Top*: Positions of the interface between two half-spaces and receiver in the grid $h \times h \times h$ (left column) and grid $H \times H \times H$ (right column), shown schematically in one vertical grid plane. *Bottom*: Comparison of three solutions. (1) Our FD for the grid $h \times h \times h$, where $h = \lambda_{\min}/6$; (2) our FD for the grid $H \times H \times H$, where $H = \lambda_{\min}/18$; (3) DWN. Note that the standard spatial sampling, that is, $h = \lambda_{\min}/6$, gives the same solution as the three times finer (and sufficiently oversampling) grid. Both FD solutions agree very well with the DWN solution.

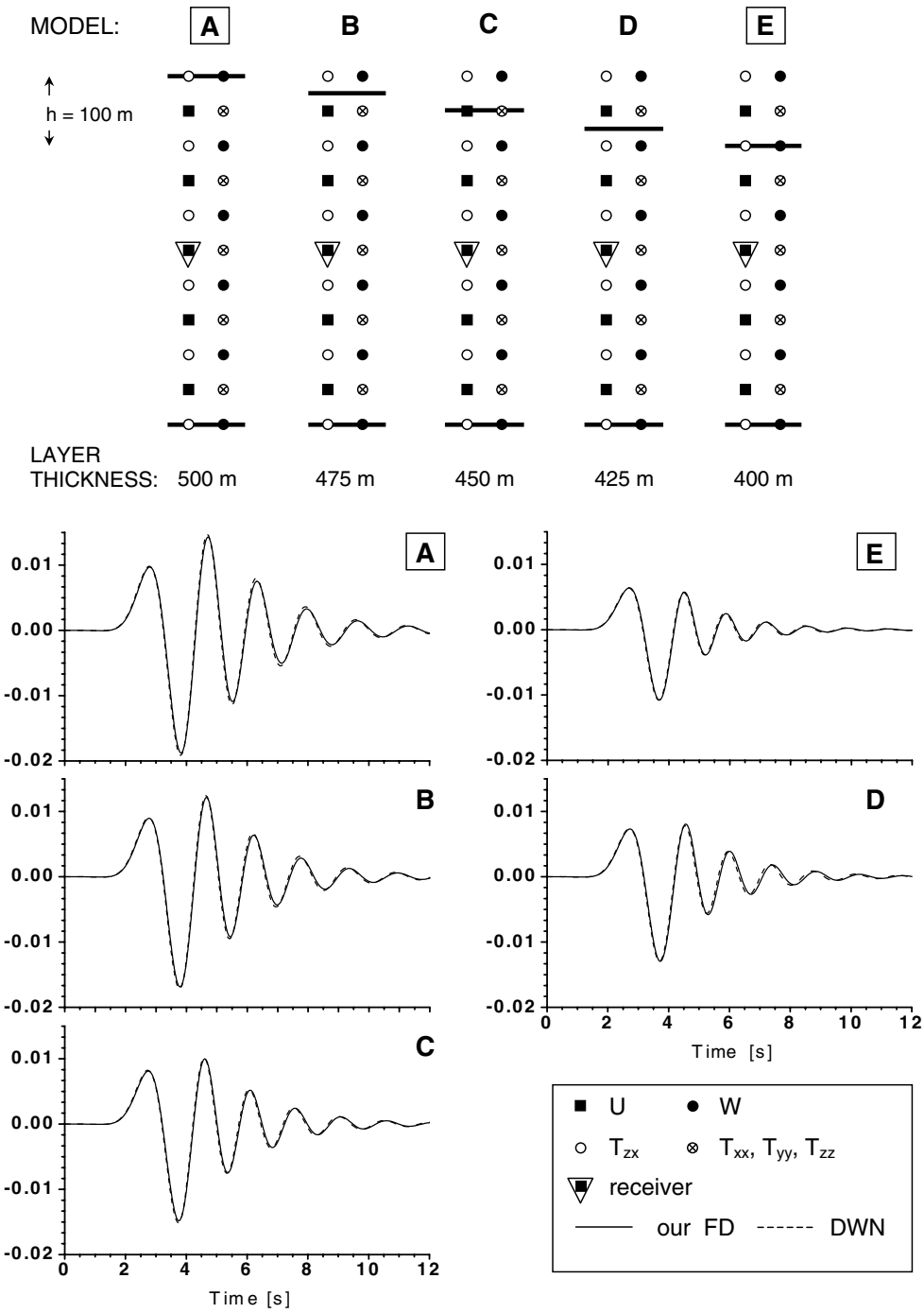

Figure 6. *Top*: Positions of the upper and lower layer–half-space interfaces in five models of a layer between two half-spaces, shown schematically in one vertical grid plane. The five models differ from each other by position of the upper layer–half-space interface in the spatial grid (the same for all models) and thus by the layer thickness. (For the parameters of the models see Table 3.) *Bottom*: Comparison of our FD and DWN synthetics for the five models. Note very good accuracy of the FD synthetics for any position of the layer–half-space interface with respect to the spatial grid. Also note considerable differences between synthetics due to variations in the layer thickness that are smaller than one grid spacing.

Table 3
Model Parameters: Interior Layer

	All Models A–E α (m/sec)		β (m/sec)		ρ (kg/m^3)
Layer	1125		625		1600
Half-spaces	5468		3126		1800
	A	B	C	D	E
Layer thickness (m)	500	475	450	425	400

α, P-wave velocity; β, S-wave velocity; ρ, density.

-900) m in the Cartesian (x,y,z) coordinate system. The lower layer–half-space interface is the plane $z = -650$ m, and the upper layer–half-space interface is the plane $z = z_i$; $z_i \in \{-1000, -1025, -1050, -1075, -1100\}$ m.

The numbers of grid cells in the x, y, and z directions were $MX = 352$, $MY = 352$, and $MZ = 620$, respectively. The spatial grid spacing was $h = 100$ m, time step $\Delta t = 0.009$ sec, and the frequency up to which the computation should be sufficiently accurate (assuming six grid spacing per minimum wavelength) was $f_{ac} = 1.04$ Hz.

The FD and DWN synthetics (U component) are compared in Figure 6. It is clear from the figure that the FD and DWN synthetics agree very well regardless of the position of the upper layer–half-space interface with respect to the spatial grid. Let us note that parameterization suggested by Graves (1996) only allows one to consider models A and E in which the upper interface is located at the grid plane with shear stress-tensor components.

It is also clear from Figure 6 that differences in thickness of the layer—smaller than one grid spacing—cause considerable changes in seismic motion. This underlines the need of a sufficiently accurate FD scheme.

Interface Oblique to a Grid Plane. In the previous numerical example the layer–half-space interfaces were coinciding or ran parallel with the horizontal grid planes. It is therefore reasonable to test the accuracy of our FD scheme in a case where the interfaces are not parallel with the grid planes. Consider physically the same interior layer between two half-spaces as in the case A (500 m thick) of the previous example but rotate it by 5° about the x axis and by 10° about the y axis. Thus, the planar layer–half-space interfaces are oblique to the grid planes (see the upper part of Fig. 7). The source is the same as in the previous example. The grid coordinates of the source and receiver are $I = 175$, $K = 175$, $L = 308$, and $I = 188$, $K = 174$, $L = 298$, respectively. The lower part of Figure 7 shows three solutions for the U-component of displacement: (1) the DWN solution (with the source and displacement components rotated so that the exact comparison with the FD solution is possible), (2) the solution obtained by our FD scheme, and (3) the FD solution assuming homogeneous cells (i.e., rather common parameterization in which one cell is characterized by only three material parameters: ρ, λ, and μ). It is clear that there is good agreement between the DWN and our FD scheme, whereas common-parameterization FD scheme gives a considerably different result.

Surface Layer over Half-Space

A single horizontal homogeneous layer is located on a homogeneous half-space. We considered two different thicknesses of the layer. In one model, the layer–half-space interface is located at a grid plane with normal stress-tensor components, in the other at a grid plane with shear stress-tensor components (see the upper part of Fig. 8). The parameters of the models are given in Table 4. The source time function as well as the focal mechanism were the same as in the case of the interior layers (see Table 2). The source was located below the layer. A receiver was located at the free surface. The coordinates of the source were (0,0,550) m; coordinates of the receiver were (1475,0,0) m, and the layer–half-space interface is the plane $z = z_i$; $z_i \in \{200,225\}$ m. The numbers of grid cells in the x, y, and z directions were $MX = 736$, $MY = 736$, and $MZ = 620$, respectively. The spatial grid spacing was $h = 50$ m, time step $\Delta t = 0.0045$ sec. Note that grid spacing is half that used in the case of the interior layers although the velocities are the same. We did this to minimize the inaccuracy in modeling the free surface.

The FD and DWN synthetics (U component) are compared in Figure 8. The FD synthetics are in very good agreement with the DWN synthetics for both models. Let us stress the large difference between seismic motions in the two models despite the fact that they differ from one another by 25 m in the layer thickness, that is, by half of the grid spacing. This again underlines the importance of having a FD scheme sensitive enough to heterogeneity of medium.

Surface Layer with a Velocity Gradient

In order to test accuracy of the scheme in the case of a velocity gradient we considered a model of a surface layer in which both the P- and S-wave velocities linearly increase with depth. The parameters of the model are in Table 5. The source time function and the focal mechanism were the same as in the previous model. The source was below the layer and its coordinates were (0,0,675) m. The receiver was located at the free surface and its coordinates were (1450,0,25) m. For the position of the layer and receiver in the grid, see the upper part of Figure 9. The numbers of grid cells in the x, y, and z directions were $MX = 736$, $MY = 736$, and $MZ = 620$, respectively. The spatial grid spacing was $h = 50$ m, time step $\Delta t = 0.0045$ sec.

The FD and DWN synthetics (U component) are compared in Figure 9. They are again in very good agreement.

Moon Valley

Sánchez-Sesma and Luzón (1995) presented computations for a 3D alluvial valley with geometry shown in Figure 10 and parameters in Table 6. The wave field was excited by a vertical incidence of a plane SV wave with a source time function (corresponding to displacement) given by

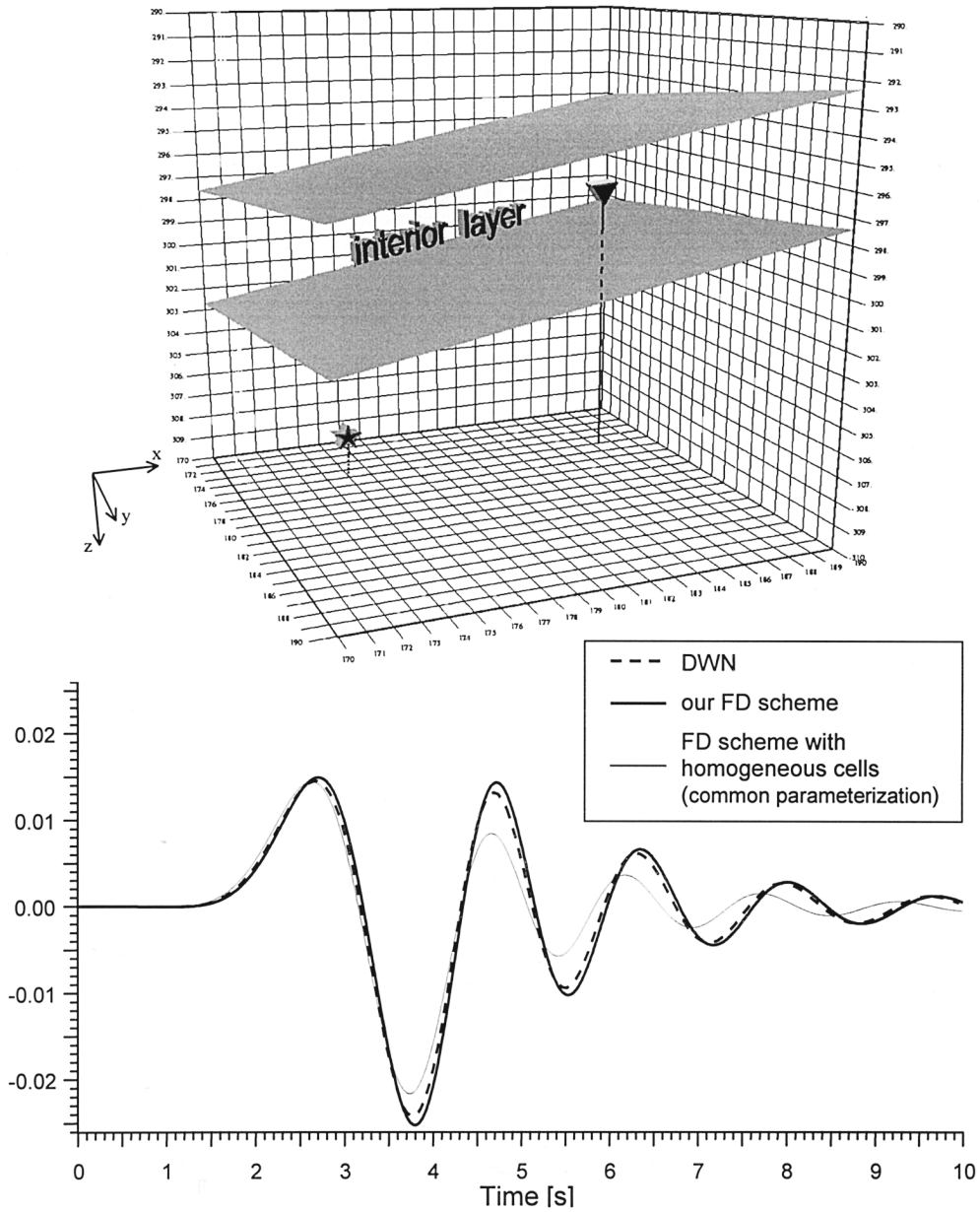

Figure 7. *Top*: Position of the layer–half-space interfaces in the model of a layer between two half-spaces. The model is physically the same as the model A shown in Figure 6. The layer is however rotated and the interfaces are oblique to the grid planes. *Bottom*: Comparison of our FD scheme with the DWN and common-parameterization FD scheme. There is good agreement between our FD and DWN synthetics while the other FD solution is considerably different.

Ricker signal, $s(t) = (\sqrt{\pi}/2)\ (\gamma - 0.5)\ e^{-\gamma}$; $\gamma = (\pi(t - t_s)/t_p)^2$, where $t_p = 3$ sec and $t_s = 1.1 \cdot t_p$. Fifty-one receivers were equidistantly distributed along the profile (see Fig. 10) at the free surface. Grid with $MX = 223$, $MY = 223$, and $MZ = 139$, grid spacing $h = 160$ m, and time step $\Delta t = 0.02$ sec were used in our FD computation. The FD synthetics are compared with those obtained with the simplified indirect boundary-element method (siBEM) by Sánchez-Sesma and Luzón (who kindly provided their solution in a digital form), see Figure 11. We can see in the figure a good level of agreement between the two solutions, though the siBEM synthetics are not sufficiently finely sampled in the time domain and display slight noncausal arrivals.

Conclusions

We considered the problem of a heterogeneous formulation of the equation of motion and the corresponding heterogeneous FD scheme for medium with a material discontinuity. We analyzed 1D and 3D problems.

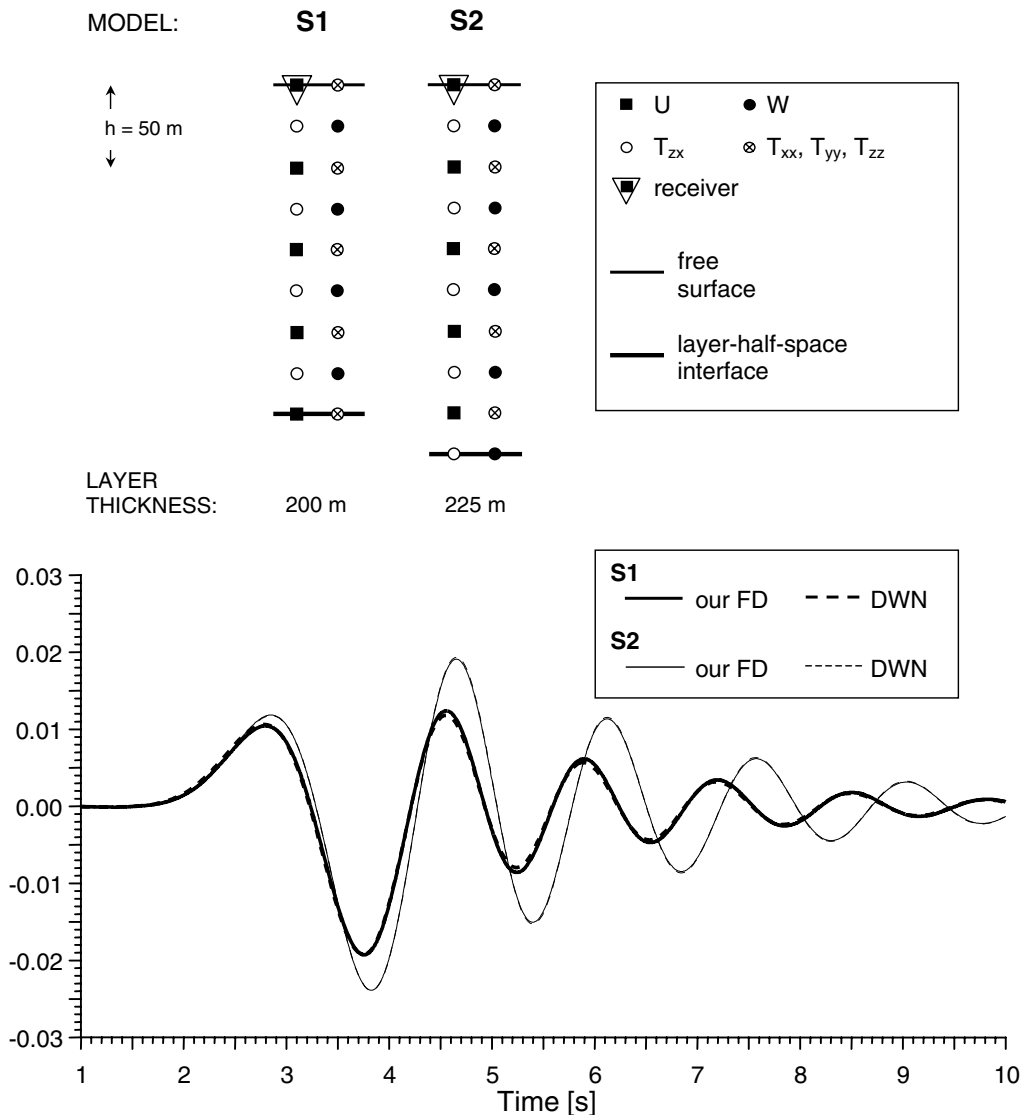

Figure 8. *Top*: Positions of the free surface and layer–half-space interface in two models of a surface layer over halfspace, shown schematically in one vertical grid plane. The two models differ from each other by position of the layer-halfspace interface in the spatial grid (the same for both models) and thus by the layer thickness. (For the parameters of the model see Table 4.) *Bottom*: Comparison of our FD and DWN synthetics for the two models. Note very good accuracy of the FD synthetics for both positions of the layer–half-space interface with respect to the spatial grid. Also note considerable difference between synthetics due to variation in the layer thickness equal to half grid spacing.

Table 4
Model Parameters: Surface Layer over Half-Space

Both Models S1 and S2	α (m/sec)	β (m/sec)	ρ (kg/m^3)
Layer	1125	625	1600
Half-space	5468	3126	1800
Layer thickness (m)	S1, 200	S2, 225	

α, *P*-wave velocity; β, *S*-wave velocity; ρ, density.

Table 5
Model Parameters: Surface Layer with a Velocity Gradient

	α (m/sec)	β (m/sec)	ρ (kg/m^3)
Layer	1125–1800	625–1000	1600
Half-space	5468	3126	1800
Layer thickness (m)	300		

α, *P*-wave velocity; β, *S*-wave velocity; ρ, density.

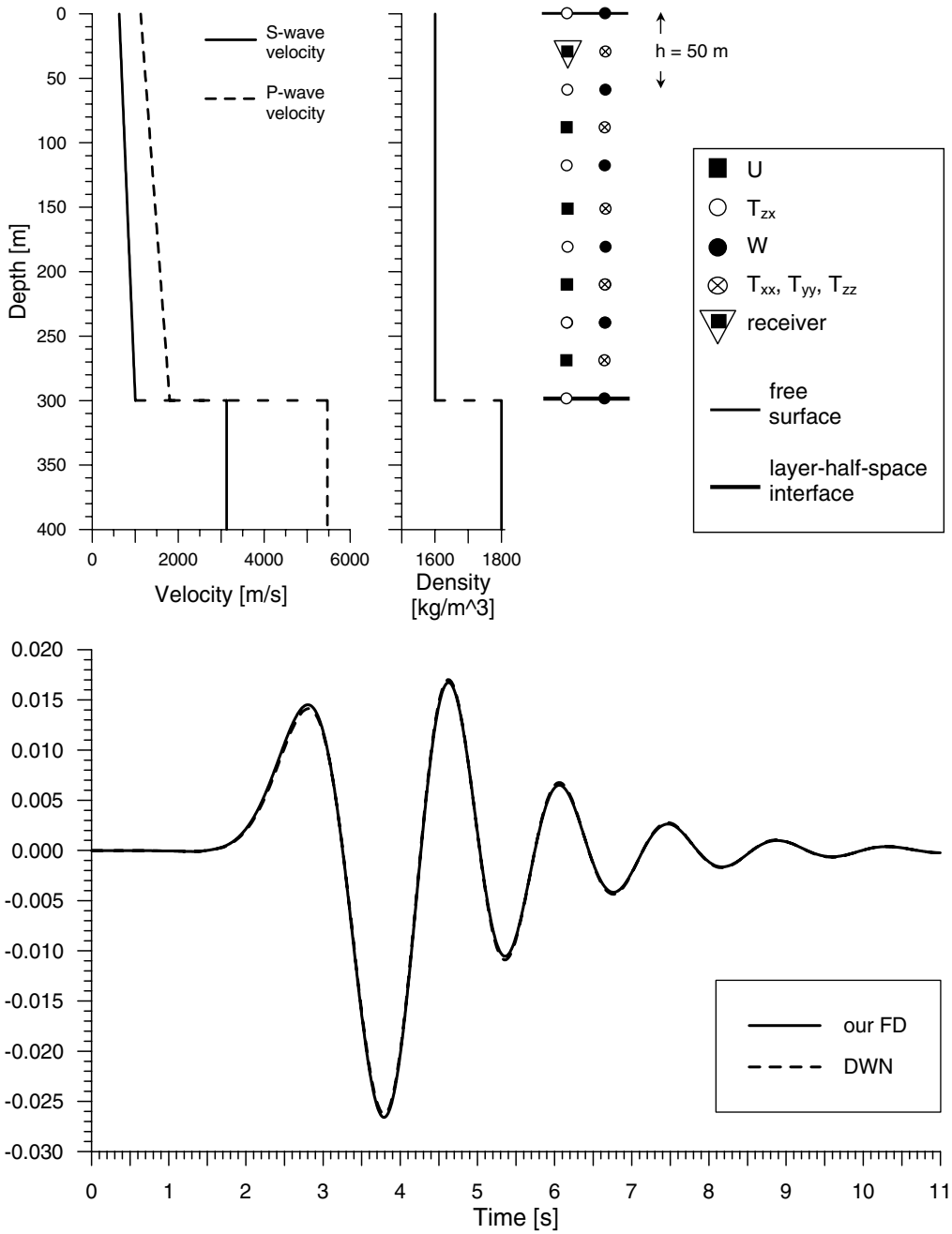

Figure 9. *Top*: Position of the layer and receiver shown schematically in one vertical grid plane. *S*-wave and *P*-wave velocities, and density in the layer and half-space. (For the parameters of the model see Table 5.) *Bottom*: Comparison of our FD and DWN synthetics. Synthetics computed by both methods agree very well.

In the 1D problem for a welded planar interface of two media, we found a simple physical model of the contact of two media and the exact heterogeneous formulation of the equation of motion and Hooke's law, that is, equations for an averaged medium representing the contact. Then we constructed a corresponding 1D heterogeneous FD scheme.

In the 3D problem we considered three cases: (1) a planar-interface contact of two isotropic media with the interface parallel to a coordinate plane in the Cartesian coordinate system, (2) a planar-interface contact with the interface in general position, and (3) a nonplanar-interface contact of two isotropic media. Five independent elastic coefficients are necessary to describe the averaged medium representing the planar-interface contact of two isotropic media because the averaged medium is transversally isotropic in the first case. In other words, Hooke's law for the averaged medium includes five independent elastic coefficients. In the second case, 21 generally nonzero elastic co-

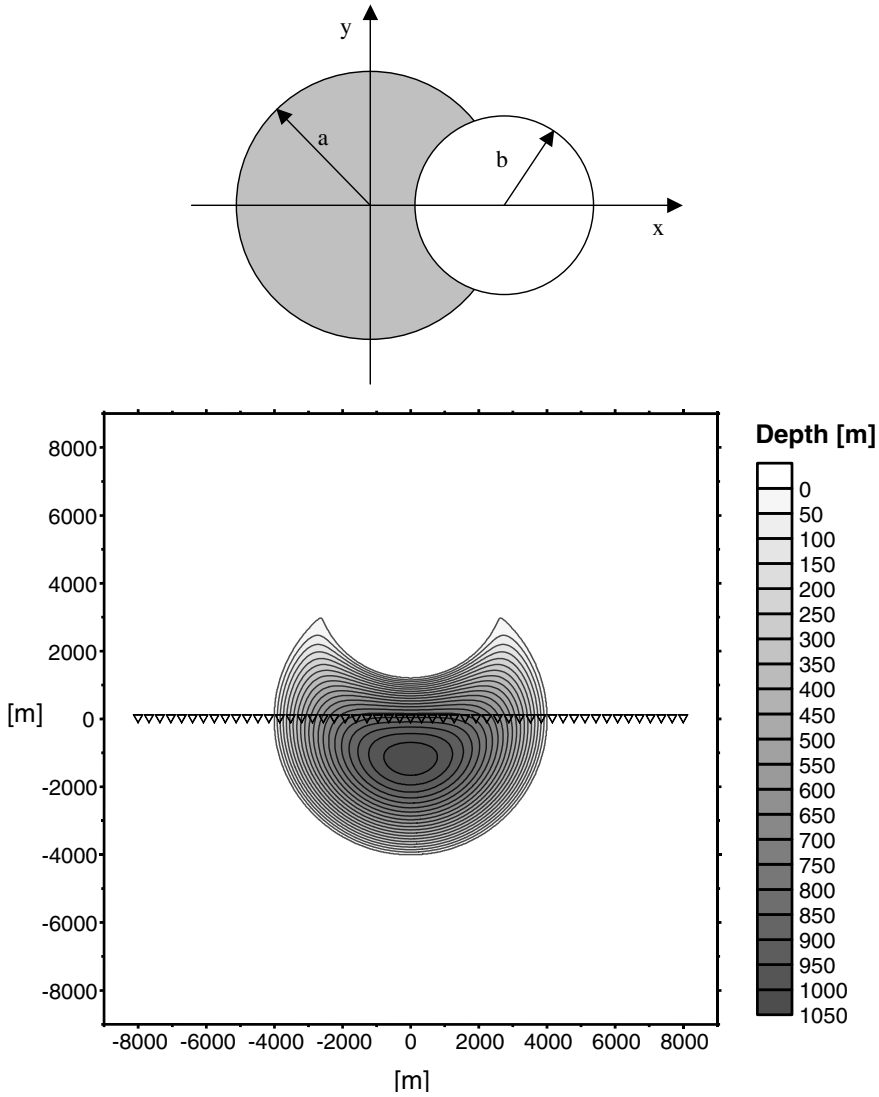

Figure 10. Geometry of the Moon Valley. *Top*: The valley is limited by two circumreferences of radii a and b; $b = 0.7a$, $a = 4000m$. Bottom: Isolines of the valley–basement interface. The horizontal line with triangles shows the profile along which the receivers were located.

Table 6
Model Parameters: Moon Valley

	α (m/sec)	β (m/sec)	ρ (kg/m^3)	Q_p	Q_s
Valley	2082	1000	1600	100	100
Basement	3464	2000	2000	∞	∞

α, P-wave velocity; β, S-wave velocity; ρ, density; Q_p, quality factor of P wave; Q_s, quality factor of S wave.

efficients are necessary to describe the averaged medium at a point of the interface. The same is true for the third case, assuming that a tangential planar interface is used at a point to approximate the nonplanar interface.

Because a corresponding heterogeneous FD scheme would require tremendous computer memory, we considered simplified boundary conditions at the contact for which the averaged medium can be described by only two elastic coefficients—as any of the two isotropic media in contact.

Based on the simplified approach we constructed the explicit heterogeneous 3D fourth-order in space, second-order in time displacement-stress FD scheme on a staggered grid with volume harmonic averaging of the bulk and shear moduli and volume arithmetic averaging of density. The scheme allows for an arbitrary position of the material discontinuity in the spatial grid.

Our displacement-stress FD scheme can be easily modified into the velocity-stress or displacement-velocity-stress FD scheme.

Numerical comparisons with the discrete-wavenumber method show that our scheme is more accurate than the staggered-grid schemes used so far.

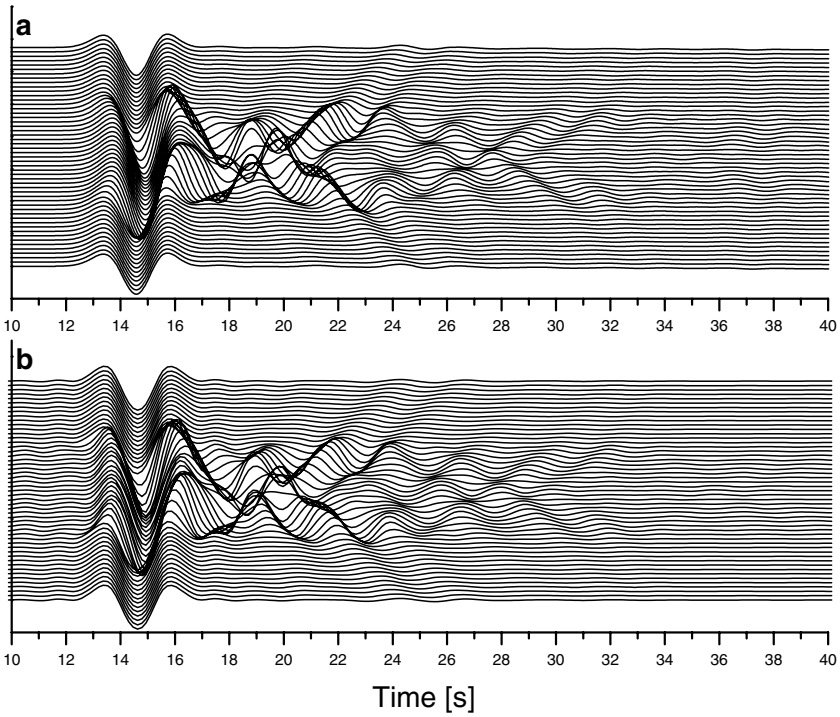

Figure 11. Comparison of the synthetics (the x component of the particle velocity) computed with (a) our FD scheme with (b) those computed by the simplified indirect boundary-element method of Sánchez-Sesma and Luzón (1995).

Numerical examples also show that differences in thickness of a layer smaller than one grid spacing can cause considerable changes in seismic motion. The results thus underline the importance of having a FD scheme with sufficient sensitivity to heterogeneity of the medium.

Acknowledgments

This work was supported in part by Grant No. 2/1090/21, VEGA, Slovak Republic; INCO-COPERNICUS Grant PL963311; European Commission Projects No. EVG1-CT-2000-00026 SESAME and No. EVG1-CT-2001-00040 EUROSEISRISK; National Science Foundation Grant CDA96-01954, and by Silicon Graphics Inc. One of the authors (P.M.) thanks the Institute for Crustal Studies, University of California at Santa Barbara, for the invitation and support. This is ICS Contribution No. 515.

References

Alterman, Z. S., and F. C. Karal (1968). Propagation of elastic waves in layered media by finite difference methods, *Bull. Seism. Soc. Am.* **58,** 367–398.

Aoi, S., and H. Fujiwara (1999). 3-D finite-difference method using discontinuous grids, *Bull. Seism. Soc. Am.* **89,** 918–930.

Boore, D. (1972). Finite-difference methods for seismic wave propagation in heterogeneous materials, in *Methods in Computational Physics*, B. A. Bolt (Editor), Vol. 11, Academic Press, New York.

Bouchon, M. (1981). A simple method to calculate Green's functions for elastic layered media, *Bull. Seism. Soc. Am.* **71,** 959–971.

Clayton, R., and B. Engquist (1977). Absorbing boundary conditions for acoustic and elastic wave equations, *Bull. Seism. Soc. Am.* **67,** 1529–1540.

Cotton, F., C. Berge, F. Lemeille, A. Pitarka, B. Lebrun, and M. Vallon (1998). Three-dimensional simulation of earthquakes in the Grenoble's basin, in *The Effects of Surface Geology on Seismic Motion*, K. Irikura, K. Kudo, H. Okada, and T. Sasatani (Editors), Vol. 2, Balkema, Rotterdam, 873–878.

Coutant, O. (1989). Program of numerical simulation AXITRA. Res. Rep. LGIT (in French), Universite Joseph Fourier, Grenoble.

Frankel, A. (1993). Three-dimensional simulations of ground motions in the San Bernardino Valley, California, for hypothetical earthquakes on the San Andreas fault, *Bull. Seism. Soc. Am.* **83,** 1020–1041.

Frankel, A., and W. Stephenson (2000). Three-dimensional simulations of ground motions in the Seattle region for earthquakes in the Seattle fault zone, *Bull. Seism. Soc. Am.* **90,** 1251–1267.

Geller, R. J., and N. Takeuchi (1998). Optimally accurate second-order time-domain finite difference scheme for the elastic equation of motion: one-dimensional case, *Geophys. J. Int.* **135,** 48–62.

Graves, R. W. (1993). Modeling three-dimensional site response effects in the Marina district basin, San Francisco, California, *Bull. Seism. Soc. Am.* **83,** 1042–1063.

Graves, R. W. (1996). Simulating seismic wave propagation in 3D elastic media using staggered-grid finite differences, *Bull. Seism. Soc. Am.* **86,** 1091–1106.

Graves, R. W., A. Pitarka, and P. G. Somerville (1998). Ground-motion amplification in the Santa Monica area: effects of shallow basin-edge structure, *Bull. Seism. Soc. Am.* **88,** 1224–1242.

Higdon, R. L. (1991). Absorbing boundary conditions for elastic waves, *Geophysics* **56,** 231–241.

Ilan, A., A. Ungar, and Z. S. Alterman (1975). An improved representation of boundary conditions in finite difference schemes for seismological problems, *Geophys. J. R. Astr. Soc.* **43,** 727–745.

Ilan, A., and D. Loewenthal (1976). Instability of finite-difference schemes due to boundary conditions in elastic media, *Geophys. Prosp.* **24,** 431–453.

Kelly, K. R., R. W. Ward, S. Treitel, and R. M. Alford (1976). Synthetic seismograms: a finite-difference approach, *Geophysics* **41,** 2–27.

Kristek, J., P. Moczo, and R. J. Archuleta (2002). Efficient methods to simulate planar free surface in the 3D 4th-order staggered-grid finite-difference schemes, *Studia Geophys. Geodet.* **46,** 355–381.

Kristek, J., P. Moczo, I. Irikura, T. Iwata, and H. Sekiguchi (1999). The 1995 Kobe mainshock simulated by the 3D finite differences, in *The Effects of Surface Geology on Seismic Motion*, K. Irikura, K. Kudo, H. Okada, and T. Sasatani (Editors), Vol. 3, Balkema, Rotterdam, 1361–1368.

Kummer, B., and A. Behle (1982). Second-order finite-difference modeling of SH-wave propagation in laterally inhomogeneous media, *Bull. Seism. Soc. Am.* **72,** 793–808.

Madariaga, R. (1976). Dynamics of an expanding circular fault, *Bull. Seism. Soc. Am.* **66,** 639–666.

Matsushima, S., H. Kawase, T. Sato, R. W. Graves, and P. G. Somerville (1998). 3D simulation of aftershocks of the Hyogo-ken Nanbu earthquake of 1995, in *The Effects of Surface Geology on Seismic Motion*, K. Irikura, K. Kudo, H. Okada, and T. Sasatani (Editors), Vol. 2, Balkema, Rotterdam, 1129–1136.

Mitchell, A. R. (1969). *Computational Methods in Partial Differential Equations*, Wiley, London.

Mizutami, H., R. J. Geller, and N. Takeuchi (2000). Comparison of accuracy and efficiency of time-domain schemes for calculating synthetic seismograms, *Phys. Earth Planet. Interiors* **119,** 75–97.

Moczo, P., M. Lucká, J. Kristek, and M. Kristeková (1999). 3D displacement finite differences and combined memory optimization, *Bull. Seism. Soc. Am.* **89,** 69–79.

Moczo, P., J. Kristek, and L. Halada (2000). 3D fourth-order staggered-grid finite-difference schemes: stability and grid dispersion, *Bull. Seism. Soc. Am.* **90,** 587–603.

Moczo, P., J. Kristek, and E. Bystrický (2001). Efficiency and optimization of the 3D finite-difference modeling of seismic ground motion, *J. Comp. Acoustics* **9,** 539–609.

Muir, F., J. Dellinger, J. Etgen, and D. Nichols (1992). Modeling elastic fields across irregular boundaries, *Geophysics* **57,** 1189–1193.

Ohminato, T., and B. A. Chouet (1997). A free-surface boundary condition for including 3D topography in the finite-difference method, *Bull. Seism. Soc. Am.* **87,** 494–515.

Olsen, K., and G. T. Schuster (1992). Seismic hazard analysis in Salt Lake Valley by finite-difference simulation of three dimensional elastic wave propagation, in *Scientific Excellence in High Performance Computing: The 1990 1BM Price Papers*, Vol. I, Sec. 6, Baldwin Press, Athens, Georgia, 135–165.

Olsen, K. B., R. J. Archuleta, and J. R. Matarese (1995). Magnitude 7.75 earthquake on the San Andreas fault: three-dimensional ground motion in Los Angeles, *Science* **270,** 1628–1632.

Olsen, K. B., R. Nigbor, and T. Konno (2000). 3D viscoelastic wave propagation in the Upper Borrego Valley, California, constrained by borehole and surface data, *Bull. Seism. Soc. Am.* **90,** 134–150.

Pitarka, A., K. Irikura, and T. Iwata (1997). Modelling of ground motion in the Higashinada (Kobe) area for an aftershock of the 1995 January 17 Hyogo-ken Nanbu, Japan, earthquake, *Geophys. J. Int.* **131,** 231–239.

Pitarka, A., K. Irikura, T. Iwata, and H. Sekiguchi (1998). Three-dimensional simulation of the near-fault ground motion for the 1995 Hyogo-ken Nanbu (Kobe), Japan, earthquake, *Bull. Seism. Soc. Am.* **88,** 428–440.

Sánchez-Sesma, F. J., and F. Luzón (1995). Seismic response of three-dimensional alluvial valleys for incident P, S, and Rayleigh waves, *Bull. Seism. Soc. Am.* **85,** 269–284.

Saenger, R. H., N. Gold, and S. A. Shapiro (2000). Modeling the propagation of elastic waves using a modified finite-difference grid, *Wave Motion* **31,** 77–92.

Schoenberg, M., and F. Muir (1989). A calculus for finely layered anisotropic media, *Geophysics* **54,** 581–589.

Sochacki, J. S., J. H. George, R. E. Ewing, and S. B. Smithson (1991). Interface conditions for acoustic and elastic wave propagation, *Geophysics* **56,** 168–181.

Takeuchi, N., and R. J. Geller (2000). Optimally accurate second order time-domain finite difference scheme for computing synthetic seismograms in 2-D and 3-D media, *Phys. Earth Planet. Interiors* **119,** 99–131.

Takenaka, H., T. Furumura, and H. Fujiwara (1998). Recent developments in numerical methods for ground motion simulation, in *The Effects of Surface Geology on Seismic Motion*, K. Irikura, K. Kudo, H. Okada, and T. Sasatani (Editors), Vol. 2, Balkema, Rotterdam, 91–101.

Virieux, J. (1984). SH-wave propagation in heterogenous media: velocity-stress finite-difference method, *Geophysics* **49,** 1933–1957.

Virieux, J. (1986). P-SV wave propagation in heterogeneous media: velocity-stress finite-difference method, *Geophysics* **51,** 889–901.

Wald, D., and R. W. Graves (1998). The seismic response of the Los Angeles Basin, California, *Bull. Seism. Soc. Am.* **88,** 337–356.

Yomogida, K., and J. T. Etgen (1993). 3-D wave propagation in the Los Angeles basin for the Whittier-Narrows earthquake, *Bull. Seism. Soc. Am.* **83,** 1325–1344.

Zahradník, J., and E. Priolo (1995). Heterogeneous formulations of elastodynamic equations and finite-difference schemes, *Geophys. J. Int.* **120,** 663–676.

Appendix

3D Fourth-Order Displacement-Stress Staggered-Grid Finite-Difference Scheme

$$
\begin{aligned}
U^{m+1}_{I,K+1/2,L+1/2} &= 2U^{m}_{I,K+1/2,L+1/2} - U^{m-1}_{I,K+1/2,L+1/2} \\
&+ \frac{\Delta^2 t}{\rho^A_{I,K+1/2,L+1/2}} F^{x,m}_{I,K+1/2,L+1/2} \\
&+ \frac{\Delta^2 t}{h} \frac{1}{\rho^A_{I,K+1/2,L+1/2}} \Big[a\Big(T^{xx,m}_{I+3/2,K+1/2,L+1/2} - T^{xx,m}_{I-3/2,K+1/2,L+1/2} \Big) \\
&\qquad + b\Big(T^{xx,m}_{I+1/2,K+1/2,L+1/2} - T^{xx,m}_{I-1/2,K+1/2,L+1/2} \Big) \\
&\qquad + a\Big(T^{xy,m}_{I,K+2,L+1/2} - T^{xy,m}_{I,K-1,L+1/2} \Big) \\
&\qquad + b\Big(T^{xy,m}_{I,K+1,L+1/2} - T^{xy,m}_{I,K,L+1/2} \Big) \\
&\qquad + a\Big(T^{zx,m}_{I,K+1/2,L+2} - T^{zx,m}_{I,K+1/2,L-1} \Big) \\
&\qquad + b\Big(T^{zx,m}_{I,K+1/2,L+1} - T^{zx,m}_{I,K+1/2,L} \Big) \Big]
\end{aligned}
$$

$$
\begin{aligned}
V^{m+1}_{I+1/2,K,L+1/2} &= 2V^{m}_{I+1/2,K,L+1/2} - V^{m-1}_{I+1/2,K,L+1/2} \\
&+ \frac{\Delta^2 t}{\rho^A_{I+1/2,K,L+1/2}} F^{y,m}_{I+1/2,K,L+1/2} \\
&+ \frac{\Delta^2 t}{h} \frac{1}{\rho^A_{I+1/2,K,L+1/2}} \Big[a\Big(T^{yy,m}_{I+1/2,K+3/2,L+1/2} - T^{yy,m}_{I+1/2,K-3/2,L+1/2} \Big) \\
&\qquad + b\Big(T^{yy,m}_{I+1/2,K+1/2,L+1/2} - T^{yy,m}_{I+1/2,K-1/2,L+1/2} \Big) \\
&\qquad + a\Big(T^{xy,m}_{I+2,K,L+1/2} - T^{xy,m}_{I-1,K,L+1/2} \Big) \\
&\qquad + b\Big(T^{xy,m}_{I+1,K,L+1/2} - T^{xy,m}_{I,K,L+1/2} \Big) \\
&\qquad + a\Big(T^{yz,m}_{I+1/2,K,L+2} - T^{yz,m}_{I+1/2,K,L-1} \Big) \\
&\qquad + b\Big(T^{yz,m}_{I+1/2,K,L+1} - T^{yz,m}_{I+1/2,K,L} \Big) \Big]
\end{aligned}
$$

$$
\begin{aligned}
W^{m+1}_{I+1/2,K+1/2,L} &= 2W^{m}_{I+1/2,K+1/2,L} - W^{m-1}_{I+1/2,K+1/2,L} \\
&+ \frac{\Delta^2 t}{\rho^{A}_{I+1/2,K+1/2,L}} F^{z,m}_{I+1/2,K+1/2,L} \\
&+ \frac{\Delta^2 t}{h} \frac{1}{\rho^{A}_{I+1/2,K+1/2,L}} \Big[a\Big(T^{zz,m}_{I+1/2,K+1/2,L+3/2} - T^{zz,m}_{I+1/2,K+1/2,L-3/2} \Big) \\
&\quad + b\Big(T^{zz,m}_{I+1/2,K+1/2,L+1/2} - T^{zz,m}_{I+1/2,K+1/2,L-1/2} \Big) \\
&\quad + a\Big(T^{zx,m}_{I+2,K+1/2,L} - T^{zx,m}_{I-1,K+1/2,L} \Big) \\
&\quad + b\Big(T^{zx,m}_{I+1,K+1/2,L} - T^{zx,m}_{L,K+1/2,L} \Big) \\
&\quad + a\Big(T^{yz,m}_{I+1/2,K+2,L} - T^{yz,m}_{I+1/2,K-1,L} \Big) \\
&\quad + b\Big(T^{yz,m}_{I+1/2,K+1,L} - T^{yz,m}_{I+1/2,K,L} \Big) \Big]
\end{aligned}
$$

$$
\begin{aligned}
T^{XX,m}_{I+1/2,K+1/2,L+1/2} &= \frac{1}{h}\Big\{ \Big(\kappa^{H}_{I+1/2,K+1/2,L+1/2} \\
&\quad + \frac{4}{3}\mu^{H}_{I+1/2,K+1/2,L+1/2} \Big) \\
&\quad \Big[a\Big(U^{m}_{I+2,K+1/2,L+1/2} - U^{m}_{I-1,K+1/2,L+1/2} \Big) \\
&\quad + b\Big(U^{m}_{I+1,K+1/2,L+1/2} - U^{m}_{I,K+1/2,L+1/2} \Big) \Big] \\
&\quad + \Big(\kappa^{H}_{I+1/2,K+1/2,L+1/2} - \frac{2}{3}\mu^{H}_{I+1/2,K+1/2,L+1/2} \Big) \\
&\quad \Big[a\Big(V^{m}_{I+1/2,K+2,L+1/2} - V^{m}_{I+1/2,K-1,I+1/2} \Big) \\
&\quad + b\Big(V^{m}_{I+1/2,K+1,L+1/2} - V^{m}_{I+1/2,K,L+1/2} \Big) \\
&\quad + a\Big(W^{m}_{I+1/2,K+1/2,L+2} - W^{m}_{I+1/2,K+1/2,L-1} \Big) \\
&\quad + b\Big(W^{m}_{I+1/2,K+1/2,L+1} - W^{m}_{I+1/2,K+1/2,L} \Big) \Big] \Big\}
\end{aligned}
$$

$$
\begin{aligned}
T^{YY,m}_{I+1/2,K+1/2,L+1/2} &= \frac{1}{h}\Big\{ \Big(\kappa^{H}_{I+1/2,K+1/2,L+1/2} \\
&\quad + \frac{4}{3}\mu^{H}_{I+1/2,K+1/2,L+1/2} \Big) \\
&\quad \Big[a\Big(V^{m}_{I+1/2,K+2,L+1/2} - V^{m}_{I+1/2,K-1,I+1/2} \Big) \\
&\quad + b\Big(V^{m}_{I+1/2,K+1,L+1/2} - V^{m}_{I+1/2,K,L+1/2} \Big) \Big] \\
&\quad + \Big(\kappa^{H}_{I+1/2,K+1/2,L+1/2} - \frac{2}{3}\mu^{H}_{I+1/2,K+1/2,L+1/2} \Big) \\
&\quad \Big[a\Big(U^{m}_{I+2,K+1/2,L+1/2} - U^{m}_{I-1,K+1/2,L+1/2} \Big) \\
&\quad + b\Big(U^{m}_{I+1,K+1/2,L+1/2} - U^{m}_{I,K+1/2,L+1/2} \Big) \\
&\quad + a\Big(W^{m}_{I+1/2,K+1/2,L+2} - W^{m}_{I+1/2,K+1/2,L-1} \Big) \\
&\quad + b\Big(W^{m}_{I+1/2,K+1/2,L+1} - W^{m}_{I+1/2,K+1/2,L} \Big) \Big] \Big\}
\end{aligned}
$$

$$
\begin{aligned}
T^{ZZ,m}_{I+1/2,K+1/2,L+1/2} &= \frac{1}{h}\Big\{ \Big(\kappa^{H}_{I+1/2,K+1/2,L+1/2} \\
&\quad + \frac{4}{3}\mu^{H}_{I+1/2,K+1/2,L+1/2} \Big) \\
&\quad \Big[a\Big(W^{m}_{I+1/2,K+1/2,L+2} - W^{m}_{I+1/2,K+1/2,L-1} \Big) \\
&\quad + b\Big(W^{m}_{I+1/2,K+1/2,L+1} - W^{m}_{I+1/2,K+1/2,L} \Big) \Big] \\
&\quad + \Big(\kappa^{H}_{I+1/2,K+1/2,L+1/2} - \frac{2}{3}\mu^{H}_{I+1/2,K+1/2,L+1/2} \Big) \\
&\quad \Big[a\Big(U^{m}_{I+2,K+1/2,L+1/2} - U^{m}_{I-1,K+1/2,L+1/2} \Big) \\
&\quad + b\Big(U^{m}_{I+1,K+1/2,L+1/2} - U^{m}_{I,K+1/2,L+1/2} \Big) \\
&\quad + a\Big(V^{m}_{I+1/2,K+2,L+1/2} - V^{m}_{I+1/2,K-1,I+1/2} \Big) \\
&\quad + b\Big(V^{m}_{I+1/2,K+1,L+1/2} - V^{m}_{I+1/2,K,L+1/2} \Big) \Big] \Big\}
\end{aligned}
$$

$$
\begin{aligned}
T^{XY,m}_{I,K,L+1/2} &= \frac{1}{h}\mu^{H}_{I,K,L+1/2} \Big[a\Big(U^{m}_{I,K+3/2,L+1/2} - U^{m}_{I,K-3/2,L+1/2} \Big) \\
&\quad + b\Big(U^{m}_{I,K+1/2,L+1/2} - U^{m}_{I,K-1/2,L+1/2} \Big) \\
&\quad + a\Big(V^{m}_{I+3/2,K,L+1/2} - V^{m}_{I-3/2,K,L+1/2} \Big) \\
&\quad + b\Big(V^{m}_{I+1/2,K,L+1/2} - V^{m}_{I-1/2,K,L+1/2} \Big) \Big]
\end{aligned}
$$

$$
\begin{aligned}
T^{ZX,m}_{I,K+1/2,L} &= \frac{1}{h}\mu^{H}_{I,K+1/2,L} \Big[a\Big(U^{m}_{I,K+1/2,L+3/2} - U^{m}_{I,K+1/2,L-3/2} \Big) \\
&\quad + b\Big(U^{m}_{I,K+1/2,L+1/2} - U^{m}_{I,K+1/2,L-1/2} \Big) \\
&\quad + a\Big(W^{m}_{I+3/2,K+1/2,L} - W^{m}_{I-3/2,K+1/2,L} \Big) \\
&\quad + b\Big(W^{m}_{I+1/2,K+1/2,L} - W^{m}_{I-1/2,K+1/2,L} \Big) \Big]
\end{aligned}
$$

$$
\begin{aligned}
T^{YZ,m}_{I+1/2,K,L} &= \frac{1}{h}\mu^{H}_{I+1/2,K,L} \Big[a\Big(V^{m}_{I+1/2,K,L+3/2} - V^{m}_{I+1/2,K,L-3/2} \Big) \\
&\quad + b\Big(V^{m}_{I+1/2,K,L+1/2} - V^{m}_{I+1/2,K,L-1/2} \Big) \\
&\quad + a\Big(W^{m}_{I+1/2,K+3/2,L} - W^{m}_{I+1/2,K-3/2,L} \Big) \\
&\quad + b\Big(W^{m}_{I+1/2,K+1/2,L} - W^{m}_{I+1/2,K-1/2,L} \Big) \Big]
\end{aligned}
$$

Nonreflecting Boundary

Nonreflecting boundary according to P.-C. Liu and R. J. Archuleta (personal comm., 2000). Consider, for example the left-hand boundary. A displacement value $U^{m+1}_{1,K,L}$ is updated as

$$
\begin{aligned}
U_{1kl}^{m+1} &= A_{01}U_{2kl}^{m+1} + A_{02}U_{3kl}^{m+1} \\
&+ A_{10}U_{1kl}^{m} + A_{11}U_{2kl}^{m} + A_{12}U_{3kl}^{m} \\
&+ A_{20}U_{1kl}^{m-1} + A_{21}U_{2kl}^{m-1} + A_{22}U_{3kl}^{m-1}
\end{aligned}
$$

where

$A_{01} = h_{1x}$
$A_{02} = 0$
$A_{10} = c_{1t} + h_{1t}$
$A_{11} = c_{xt} + h_{xt} - h_{1x}c_{1t}$
$A_{12} = -h_{1x}c_{xt}$
$A_{20} = -h_{1t}c_{1t}$
$A_{21} = -h_{xt}c_{1t} - h_{1t}c_{xt}$
$A_{22} = -h_{xt}c_{xt}$

and

$h_{1x} = (\gamma_S - bG)/B\cdot G$
$h_{1t} = (1 - bG)/B\cdot G$
$h_{xt} = b/B$
$c_{1t} = 1 - \gamma_P$
$c_{xt} = \gamma_P$
$G = 1 + \gamma_S$
$B = 1 - b$
$\gamma_S = \beta\Delta t/h$
$\gamma_P = \alpha\Delta t/h$
$b = 0.4$,

α and β being the P- and S-wave speeds, respectively.

Department of Geophysics
Faculty of Mathematics, Physics and Informatics
Comenius University
Mlynská dolina F1
842 48 Bratislava
Slovak Republic
(P.M.)

Geophysical Institute
Slovak Academy of Sciences
Dúbravská cesta 9
845 28 Bratislava
Slovak Republic
(P.M., J.K., L.H.)

Geophysical Institute
Academy of Sciences of the Czech Republic
Boční II
141 31 Praha
Czech Republic
(V.V.)

Institute for Crustal Studies
University of California at Santa Barbara
Santa Barbara, California 93106
(R.J.A.)

Manuscript received 21 May 2001.